JCI insight

RESEARCH ARTICLE

Epigenetic modulation of β cells by interferon-α via PNPT1/mir-26a/TET2 triggers autoimmune diabetes

Mihaela Stefan-Lifshitz,[1] Esra Karakose,[2] Lingguang Cui,[1] Abora Ettela,[1] Zhengzi Yi,[3] Weijia Zhang,[3] and Yaron Tomer[1]

[1]Division of Endocrinology and the Fleischer Institute for Diabetes and Metabolism, Albert Einstein College of Medicine, New York, New York, USA. [2]Diabetes, Obesity, and Metabolism Institute and [3]Department of Medicine Bioinformatics Core, Icahn School of Medicine at Mount Sinai, New York, New York, USA.

Type 1 diabetes (T1D) is caused by autoimmune destruction of pancreatic β cells. Mounting evidence supports a central role for β cell alterations in triggering the activation of self-reactive T cells in T1D. However, the early deleterious events that occur in β cells, underpinning islet autoimmunity, are not known. We hypothesized that epigenetic modifications induced in β cells by inflammatory mediators play a key role in initiating the autoimmune response. We analyzed DNA methylation (DNAm) patterns and gene expression in human islets exposed to IFN-α, a cytokine associated with T1D development. We found that IFN-α triggers DNA demethylation and increases expression of genes controlling inflammatory and immune pathways. We then demonstrated that DNA demethylation was caused by upregulation of the exoribonuclease, PNPase old-35 (PNPT1), which caused degradation of miR-26a. This in turn promoted the upregulation of ten-eleven translocation 2 (TET2) enzyme and increased 5-hydroxymethylcytosine levels in human islets and pancreatic β cells. Moreover, we showed that specific IFN-α expression in the β cells of IFNα–INS1^{CreERT2} transgenic mice led to development of T1D that was preceded by increased islet DNA hydroxymethylation through a PNPT1/TET2–dependent mechanism. Our results suggest a new mechanism through which IFN-α regulates DNAm in β cells, leading to changes in expression of genes in inflammatory and immune pathways that can initiate islet autoimmunity in T1D.

Introduction

Type I diabetes (T1D) develops when environmental triggers interact epigenetically with susceptibility genes, leading to loss of immune self-tolerance to β cell antigens and resulting in autoimmune destruction of the insulin-producing β cells (1, 2). More than 40 genetic loci have been shown to be associated with T1D risk in genome-wide association studies (GWAS) and almost 50% of the genes in these loci are expressed in human pancreatic islets and β cells (3). Many of the T1D susceptibility genes encode products involved in β cell function and survival (4, 5), as well as in β and immune cell responses to viral infections (6). Several of these T1D-associated genes have been shown to be regulated at the transcriptional level by proinflammatory cytokines, suggesting a mechanism for mediating the deleterious effects of these cytokines on β cells (5). Recent studies have also highlighted the involvement of β cell microRNAs (miRs) in the cytotoxic effect of proinflammatory cytokines on islets (7–9). In addition, the ability of β cells to produce chemokines such as CXCL10 (10, 11), CXCL1, and CXCL2 (12, 13), as well as the proinflammatory cytokine IL-1β (14, 15) may also contribute to the initiation of the autoimmune response leading to their own demise. Taken together, accumulating data support the concept of an active role of β cells in triggering the inflammatory mechanisms that activate self-reactive T cells in T1D.

Recent evidence suggests that type I interferons (IFNs) mediate the crosstalk between β cells and the immune system that initiates the autoimmune response in T1D (16, 17). Indeed, an IFN-α gene signature was detected in pancreatic islets from patients with T1D (18–20) and was shown to precede clinical onset in individuals at risk of developing T1D (21–23). Treatment with IFN-α can also induce or accelerate a diabetogenic process in patients treated with this cytokine for chronic hepatitis C, or for other conditions (24, 25). In addition, transgenic mice with constitutive overexpression of IFN-α in β cells develop T1D (26)

Conflict of interest: YT was previously (1/2015–6/2017) the PI on a basic research project jointly funded by the Juvenile Diabetes Research Foundation and Pfizer.

Submitted: December 6, 2018
Accepted: January 29, 2019
Published: March 7, 2019

Reference information:
JCI Insight. 2019;4(5):e126663.
https://doi.org/10.1172/jci.insight.126663.

and overexpression of IFN-α–regulated genes was found in 4- and 6-week-old NOD mice, prior to the onset of diabetes (27). Blocking the IFN-α receptor with a monoclonal antibody prevents T1D development in NOD and *Rip*-LCMV mouse models (27, 28). A role of IFN-α in initiating autoreactivity against β cells was also highlighted by studies showing the ability of IFN-α to mediate β cell function and survival, by promoting ER stress in β cells (29, 30). However, the molecular mechanisms by which IFN-α alters β cell gene expression and function, and promotes a diabetogenic islet environment are not fully understood.

Epigenetic regulation has been proposed as a key mechanism by which cellular and environmental factors interact with susceptibility genes to trigger T1D (31) as well as other complex diseases (32–35). Our own data in autoimmune thyroiditis showed that IFN-α can induce epigenetic changes that are key to triggering autoimmunity (36, 37). Similarly, in T1D, compelling evidence provided by several genome-scale DNA methylation (DNAm) studies in monozygotic twins point to the fundamental role of environmentally induced epigenetic changes in initiating T1D (38–41). Locus-specific DNAm of the insulin (*INS*) promoter has also been associated with T1D (42), and DNAm patterns at key genomic loci have been shown to remain stable over 16 years in T1D patients and were associated with metabolic memory (43). Recent studies have revealed that dynamic and reversible DNAm changes through epigenetic DNA modifiers, DNA methyltransferases (DNMTs), and ten-eleven translocation (TET) enzymes, can function to modulate genomic responses to a given environment (44). Moreover, epigenetic modifications due to transient exposures can have long-lasting effects, can manifest later in the development of the disease, or can be transmitted transgenerationally (45, 46).

Given the central role of β cell alterations due to virally induced cytokines, specifically type I IFNs, in initiating T1D, we hypothesized that exposure of β cells to IFN-α during viral infections can impact their epigenome and trigger an inflammatory gene expression pattern that in turn generates a diabetogenic islet microenvironment, promoting the autoimmune response. In this study, we show that IFN-α induces active DNA demethylation correlated with overexpression of inflammatory and innate immune pathway genes in human pancreatic islets. We demonstrate that IFN-α exposure causes DNA demethylation by upregulation of the exoribonuclease PNPase old-35 (*PNPT1*), which mediates degradation of miR-26a leading to overexpression of methylcytosine dioxygenase *TET2* and increased 5-hydroxymethylcytosine levels in human islets and β cells. Moreover, expression of IFN-α in pancreatic β cells of IFNα-INS1^{CreERT2} transgenic mice leads to development of T1D that is preceded by increased islet DNA hydroxymethylation through the PNPT1/TET2 mechanism. These results provide a mechanistic framework to explain how inflammatory triggers such as viral infections can modify the β cell epigenome and modulate the interactions between the immune system and β cells, to trigger autoimmunity in T1D.

Results

IFN-α induces global DNAm and increased mRNA gene expression in human pancreatic islets. To characterize DNAm changes induced by IFN-α, we exposed human pancreatic islets from 3 donors to 2,000 IU IFN-α (47) and analyzed the DNAm patterns for a total of 485,577 CpG sites, using the Infinium HumanMethylation450 BeadChip. After quality control and filtering (detection $P > 0.05$), 465,070 sites were used in our DNAm analyses. To identify differentially methylated CpG sites between IFN-α–treated and untreated samples, we performed a paired LIMMA test (37, 38). CpG sites were considered differentially methylated between IFN-α–treated and untreated islets if they exhibited a methylation level change of 10% ($P < 0.05$). We identified 2,564 hyper- and 8,963 hypomethylated sites in the IFN-α–treated compared with untreated samples (Figure 1A). Of these, 1,623 hyper- and 4,216 hypomethylated sites were annotated to gene loci. We used bisulfite sequencing to validate the results from the methylation array (SI Results and Supplemental Figure 1; supplemental material available online with this article; https://doi.org/10.1172/jci.insight.126663DS1). Most of the differentially methylated sites (62%) were located in the gene body regions, followed by regions upstream relative to the transcriptional start sites (TSS) (14% of hypo- and 18% of hypermethylated CpGs) (SI Results and Supplemental Figure 2). Overall, we identified significantly more hypomethylated CpG sites (71.8%) than hypermethylated sites (28.2%) in IFN-α–treated versus untreated samples (Figure 1A). Gene Ontology (GO) analysis of the hypomethylated genes showed overrepresentation of genes in pathways of fatty acid oxidation, protein phosphorylation, gene regulation, and apoptosis (Supplemental Table 1).

Next, we assessed the effect of IFN-α on gene expression in human islets by RNA sequencing (RNA-seq). To identify differentially expressed genes, we performed DEGseq analysis comparing each paired

IFN-α–treated and untreated islets. Using an FDR less than 5% and a fold change cutoff of 1.5 or greater, we identified 487 differentially expressed transcripts in all IFN-α–treated islets compared with paired untreated islets. Of these 487 genes, 441 were upregulated and only 46 downregulated in IFN-α–treated islets ($P < 0.01$) (Figure 1B). GO analysis of the IFN-α–upregulated genes showed an overrepresentation of genes within pathways directly related to the innate or adaptive immune system: immune response ($P < 1.102 \times 10^{-23}$), response to virus ($P < 1.812 \times 10^{-20}$), and antigen processing and presentation ($P < 1.528 \times 10^{-11}$) (Supplemental Table 2). Similarly, ingenuity pathway analysis (IPA) identified pathways and gene interaction networks that were centered on IFN regulatory factors (IRFs), *STAT* and *NF-kB* transcriptional regulators, and included genes associated with antiviral activity and inflammatory and immune responses (Supplemental Table 3 and Supplemental Figure 3). Upregulation of key representative genes from these pathways, including *OAS1*, *SP100*, *IFIH1*, *CD40*, *TLR3*, and *IRS1*, was confirmed by qRT-PCR (Supplemental Figure 4). Additionally, we used the IPA upstream regulator analysis to predict transcriptional regulators associated with gene expression patterns induced by IFN-α in human islets. Members of the IRF and STAT transcription factor families were identified as upstream regulators of the IFN-α–upregulated transcripts, with *IRF7* predicted to control most of the transcripts in the data set (Supplemental Table 4).

Because DNA hypomethylation is expected to activate gene transcription we next explored the relationship between genes that were significantly hypomethylated by IFN-α and genes whose mRNA expression levels were significantly induced by IFN-α in pancreatic islets. Fifty-six out of 441 IFN-α–upregulated genes also showed decreased DNAm (Figure 1C and Supplemental Table 5). We then used DAVID functional annotation analysis (https://david.ncifcrf.gov/) to test whether genes in biological pathways that showed increased mRNA expression induced by IFN-α were also enriched among the hypomethylated genes in IFN-α–treated islets. Genes in immune ($P < 2.24 \times 10^{-08}$), antiviral ($P < 3.47 \times 10^{-07}$), and inflammatory ($P < 7.92 \times 10^{-07}$) pathways were both upregulated at the transcriptional level by IFN-α as well as hypomethylated by IFN-α (Figure 1D and Supplemental Table 6). Taken together, these results suggest that in human pancreatic islets, IFN-α induces upregulation of inflammatory and innate immune genes, in parallel with significantly higher DNA hypomethylation of these genes.

IFN-α affects TET gene expression and DNA hydroxymethylation. We next sought to determine the mechanism by which IFN-α induces DNA hypomethylation in pancreatic islets. Because DNA replication does not occur in cultured pancreatic islets, we investigated whether the DNA hypomethylation was caused by active DNA demethylation in IFN-α–treated islets. Thus, we measured the expression of the enzymes that control active DNA demethylation: *TET* and thymine-DNA glycosylase (*TDG*), as well as DNMTs (*DNMT3A* and *DNMT3B*) (48). We analyzed mRNA levels of *TET* (*TET1*, *TET2*, and *TET3*) and *TDG* genes in human islets (as indicated in individual experiments below) treated with IFN-α, compared with untreated islets. Expression levels of *TET1/2/3* and *TDG* genes were significantly upregulated in the IFN-α–treated islets. IFN-α increased *TET2* expression the most, upregulating its levels 1.8-fold relative to untreated islets ($P < 1.36 \times 10^{-07}$, $n = 28$); followed by *TET3*, with a 1.5-fold change ($P < 0.005$, $n = 16$); *TDG*, 1.4-fold change ($P < 0.007$, $n = 23$); and *TET1*, 1.3-fold change ($P < 0.05$, $n = 17$) (Figure 2A). In addition, mRNA levels of *Tet1/2/3* were upregulated in NIT-1, a mouse β cell line, 24 and 48 hours after IFN-α treatment (Supplemental Figure 5). We also assessed mRNA levels of *DNMT3A* and *DNMT3B*, two enzymes involved in both de novo methylation and active demethylation of DNA (49). *DNMT3A* levels were upregulated by 1.28-fold in IFN-α–treated islets ($P = 0.003$, $n = 12$), while *DNMT3B* levels were not affected by IFN-α treatment ($P = 0.11$, $n = 11$) (Supplemental Figure 6).

TET proteins mediate active DNA demethylation by hydroxylation of 5-methylcytosine (5mC) to 5-hydroxymethylcytosine (5hmC), which is further converted to unmodified cytosine through sequential events (50). Thus, we assessed TET hydroxylase activity in nuclear extracts from 7 islets treated or not with IFN-α, by quantifying TET-hydroxymethylated products. We found significant variability in TET activity in untreated islets (Supplemental Figure 7A); this baseline variability is likely due to differences in cellular activities known to interfere with TET's hydroxylase activity between individual islet samples (e.g., changes in cellular reactive oxygen species levels or Krebs cycle metabolites) (51–53). However, despite the baseline variability, IFN-α increased TET activity compared with baseline in all samples. Overall, IFN-α treatment of islets increased TET activity by 1.3-fold (Figure 2B and Supplemental Figure 7A).

To confirm these findings, we measured 5hmC levels in genomic DNA from islets treated with IFN-α for 24 and 48 hours. IFN-α treatment for 24 hours increased the percentage of 5hmC by 2-fold, from 0.1% 5hmC in control islets to 0.2% 5hmC in IFN-α–treated islets (Figure 2C and Supplemental Figure 7B).

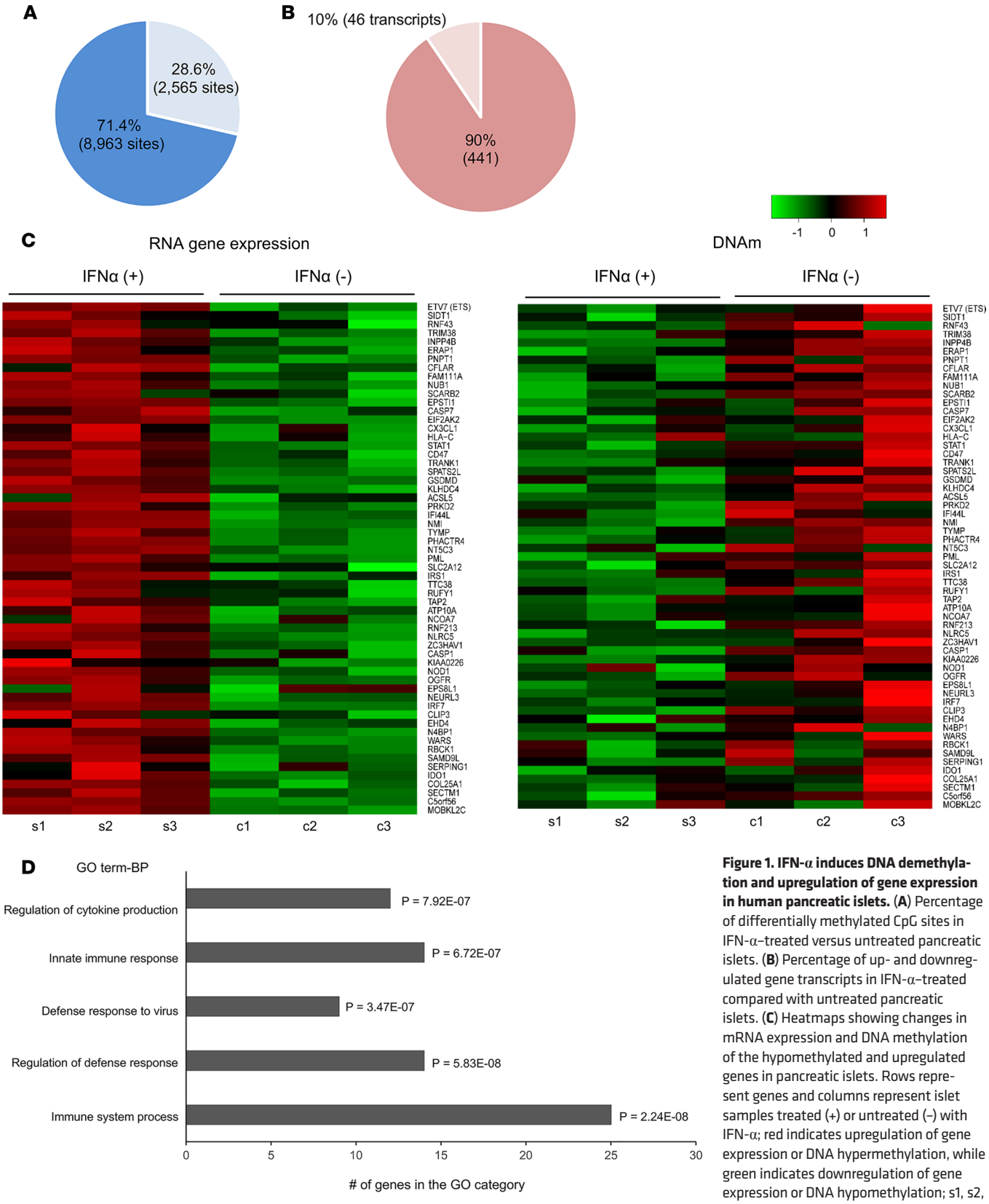

Figure 1. IFN-α induces DNA demethylation and upregulation of gene expression in human pancreatic islets. (**A**) Percentage of differentially methylated CpG sites in IFN-α–treated versus untreated pancreatic islets. (**B**) Percentage of up- and downregulated gene transcripts in IFN-α–treated compared with untreated pancreatic islets. (**C**) Heatmaps showing changes in mRNA expression and DNA methylation of the hypomethylated and upregulated genes in pancreatic islets. Rows represent genes and columns represent islet samples treated (+) or untreated (–) with IFN-α; red indicates upregulation of gene expression or DNA hypermethylation, while green indicates downregulation of gene expression or DNA hypomethylation; s1, s2, and s3 indicate IFN-α–treated samples and c1, c2, and c3 indicate untreated controls. (**D**) Top Gene Ontology (GO) terms based on biological processes (BP) overrepresented in the group of genes with increased mRNA expression and DNA hypomethylation.

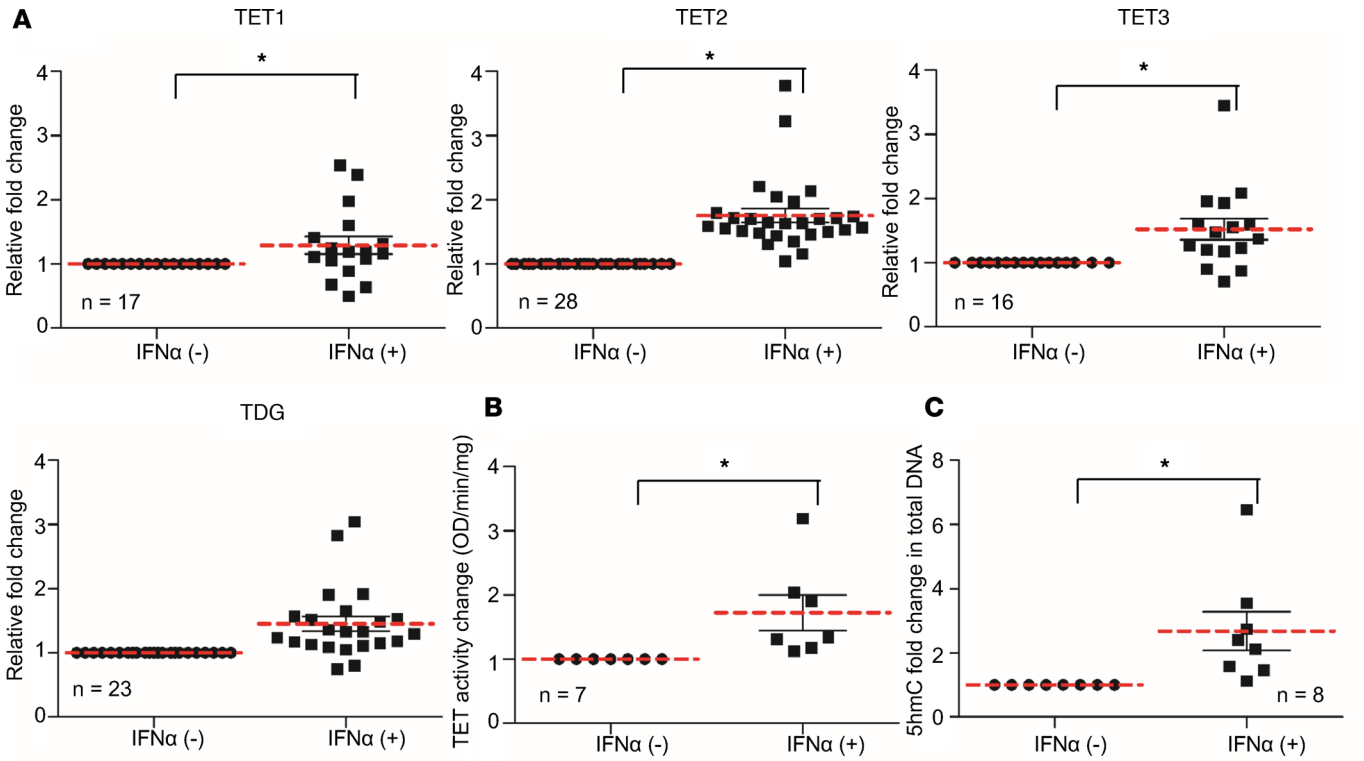

Figure 2. IFN-α causes active DNA demethylation by upregulation of TET enzyme expression and global DNA hydroxymethylation. (**A**) qRT-PCR analysis of *TET1/2/3* and *TDG* expression in islets treated (+) and untreated (–) with IFN-α. (**B**) Quantification of TET hydroxylase activity in nuclear extracts from islets treated or not with IFN-α, through detection of the TET-converted hydroxymethylated products. (**C**) Quantification of 5-hydroxymethylcytosine (5hmC) in genomic DNA from islets treated and untreated with IFN-α. For **A**–**C**, results are presented as fold change of IFN-α–treated relative to untreated islets that were considered having a fold-change of 1; squares and circles represent individual islet samples treated and untreated with IFN-α, respectively; dotted horizontal lines represent the median fold level; differences between IFN-α–treated and untreated samples were determined by *t* test. $^*P < 0.05$.

IFN-α treatment for 48 hours further increased the percentage of 5hmC (Supplemental Figure 7C). These results suggested that IFN-α induces DNA demethylation in islets via conversion of 5mC to 5hmC by upregulating TET proteins, in particular TET2.

Upregulation of TET2 in IFN-α–treated islets is mediated by miR-26a. Because *TET2* mRNA levels were the most upregulated in IFN-α–treated islets, we investigated the regulatory mechanisms by which IFN-α upregulated TET2 expression and activity. Several miRs are known to regulate *TET2* expression (54, 55); therefore, we tested if the expression levels of these miRs were altered by IFN-α. We tested 5 miRs that were previously shown to regulate 5hmC levels by directly binding to the *TET2* 3′-UTR: miR-22, miR-26a, miR-29b, miR-101, and miR-125b (55). Figure 3A shows the specific binding sites for each of these miRs (as predicted by TargetScan) to the human and mouse *TET2* 3′-UTR. To test whether the selected miRs target the *TET2* 3′-UTR in β cells, we cotransfected a luciferase (Luc) plasmid containing the 3′-UTR of human *TET2* along with the mimics for all 5 candidate miRs into the NIT-1 cells. As expected, all tested miRs targeted the *TET2* 3′-UTR; 4 of the tested miRs (miR-26a, miR-29b, miR-101, and miR-125b) decreased Luc expression by more than 30%, while miR-22 reduced Luc expression by 12% in NIT-1 cells (Figure 3B).

To test whether IFN-α suppressed the miR effects on *TET2* expression we cotransfected the pTET2-3′-UTR Luc plasmid together with the mimics of the 5 miRs into IFN-α–treated and untreated NIT-1 cells. IFN-α treatment downregulated miR-26a activity, causing a significant increase in Luc expression (increase of 111%, $P < 0.006$). IFN-α had less pronounced effects on miR-22 and miR-29b, increasing Luc expression by 17% ($P < 0.03$) and 26% ($P < 0.007$), respectively. miR-125b and miR-101 activities were not affected by IFN-α (Figure 3C).

Because the effect of IFN-α on miR-26a was the most robust, we directly assessed the role of IFN-α in miR-26a–mediated regulation of *TET2* at the RNA level in NIT-1 cells. We transfected IFN-α–treated and untreated NIT-1 cells with miR-26a mimic and inhibitor, and analyzed their effects on miR-26a and *TET2* expression. IFN-α treatment of cells transfected with miR-26a mimic significantly decreased miR-26a levels

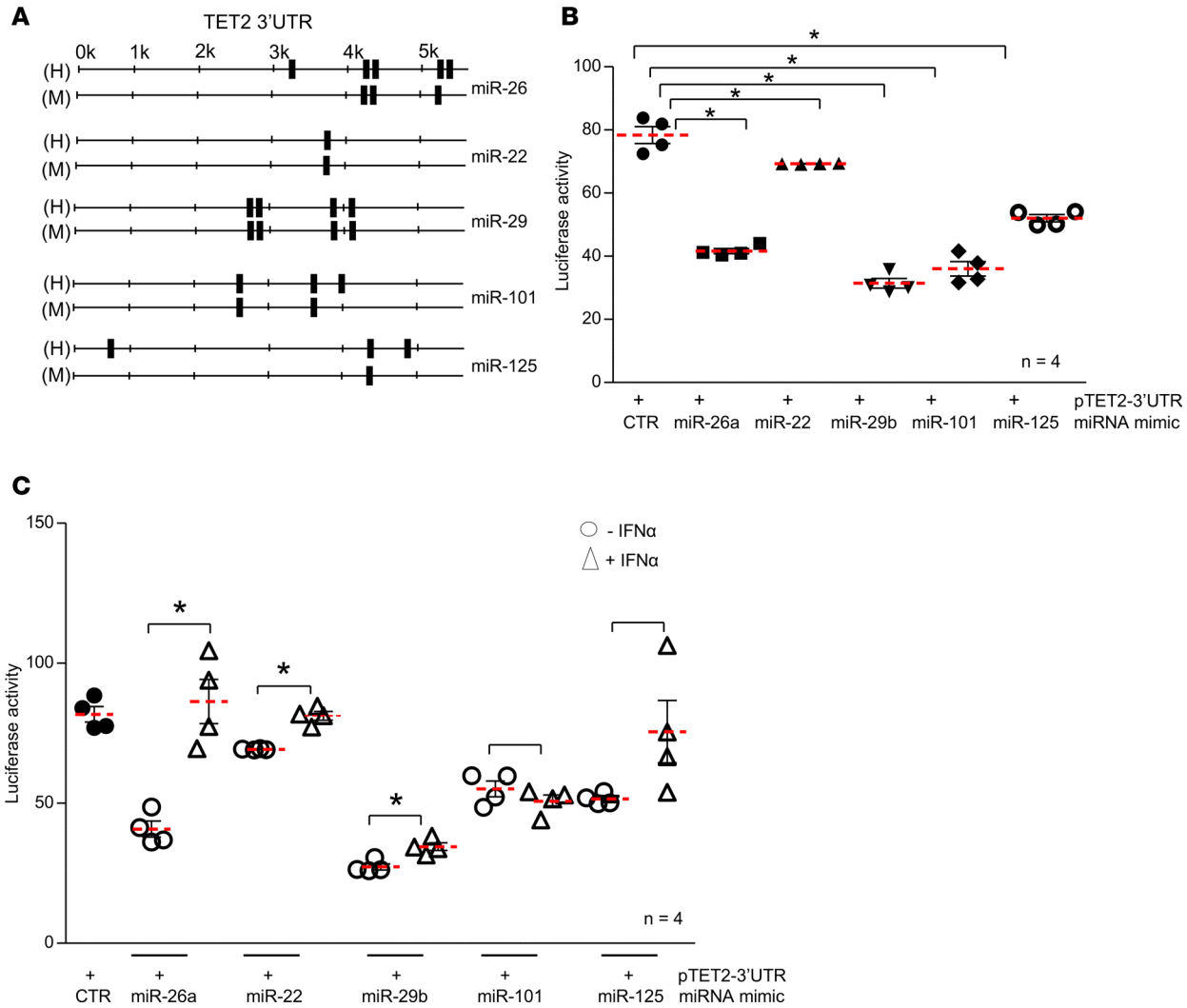

Figure 3. IFN-α regulates TET2 expression through specific miRs. (**A**) Key TET2-targeting miRs predicted by TargetScan for human and mouse. Vertical black bars, miR sites; H, human; M, mouse. (**B**) Relative luciferase activity in NIT-1 cells cotransfected with pTET2-3′-UTR constructs and TET2-targeting miR mimics: miR-26a, miR-22, miR-29b, miR-101, and miR-125. Negative control samples were cotransfected with pTET2-3′-UTR and a control miR mimic. (**C**) Relative luciferase activity in IFN-α–treated and untreated NIT-1 cells cotransfected with pTET2-3′-UTR constructs and TET2-targeting miRs. For **B** and **C**, data are representative of 4 independent experiments; results are presented as fold change of quadruplicate samples ± SD; differences between control and samples transfected with pTET2-3′-UTR and miR mimic were determined by *t* test. **P* < 0.05.

(*P* < 0.006) and increased *TET2* mRNA expression (*P* < 0.05), compared with untreated cells (Figure 4A). Moreover, miR-26a was downregulated in NIT-1 cells after both 24 and 48 hours of IFN-α treatment (Supplemental Figure 8). Upregulation of TET2 in IFN-α–treated NIT-1 cells transfected with miR-26a mimic was also confirmed at the protein level (Figure 4B). In contrast, IFN-α augmented the effect of the miR-26a inhibitor in reducing miR-26a expression (*P* < 0.006) and increasing *TET2* expression (*P* < 0.005) (Figure 4C). These results demonstrate that IFN-α upregulates TET2 expression by suppressing miR-26a.

To examine whether IFN-α has the same effects in human cells we tested the effects of IFN-α on human islets. Indeed, supporting the results in NIT-1 cells, we showed that the expression of mature miR-26a was downregulated in 22 IFN-α–treated human islets, compared with untreated islets (*P* < 0.005) (Figure 4D). In addition, we found that IFN-α treatment triggered downregulation of miR-22 (*P* = 0.02) and miR-29b (*P* = 0.04), while miR-101 and miR-125b remained unchanged in human islets (SI Results and Supplemental Figure 9A).

Next we analyzed whether the mechanisms by which IFN-α regulates miR-26a expression involved decreased transcription of miR-26a, or increased degradation of miR-26a. We measured the expression of primary miR-26a transcripts in 13 human islets treated or not treated with IFN-α. miR-26a is transcribed

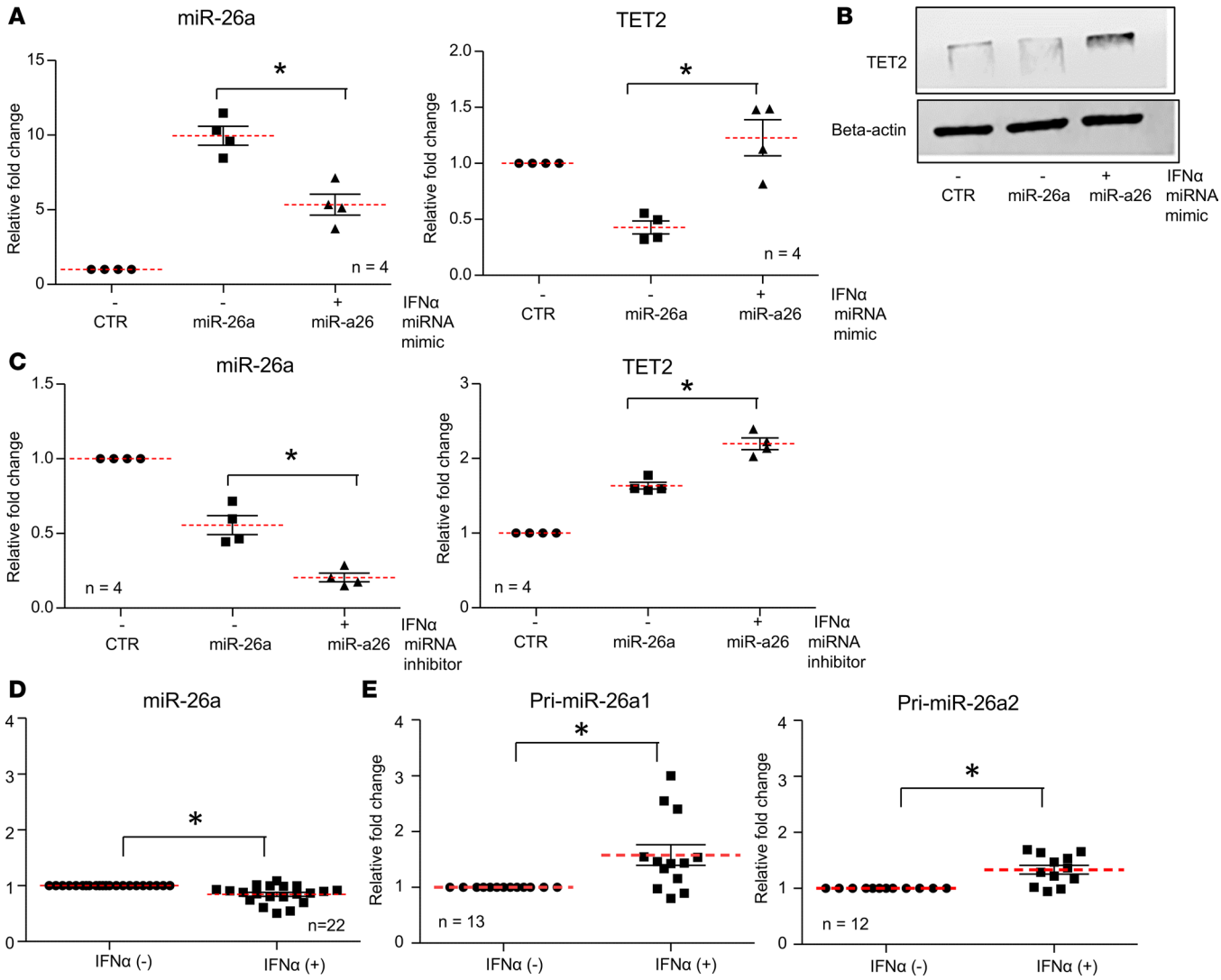

Figure 4. IFN-α upregulates TET2 by inhibiting mature miR-26a expression. (**A**) qRT-PCR analysis of miR-26a and *TET2* expression in IFN-α–treated and untreated NIT-1 cells transfected with miR-26a mimic. (**B**) TET2 protein detected by immunoblot in IFN-α–treated and untreated NIT-1 cells transfected with miR-26a mimic. β-Actin was used as control. (**C**) qRT-PCR analysis of miR-26a and *TET2* in IFN-α–treated and untreated NIT-1 cells transfected with miR-26a inhibitor. For **A** and **C**, data are representative of 3 independent experiments; results are presented as fold change of quadruplicate samples ± SD. (**D**) Relative expression levels of mature miR-26a in human islets treated and untreated with IFN-α assessed by qRT-PCR. (**E**) qRT-PCR of primary miR-26a (pri-miR-26a-1 and pri-miR-26a-2) in IFN-α–treated relative to untreated islets. For **D** and **E**, squares and circles represent individual islet samples treated and untreated with IFN-α respectively; dotted horizontal lines represent the median fold level. For **A**–**E**, differences between controls and different constructs and between IFN-α–treated and untreated islets were determined by *t* test for independent samples. $^*P < 0.05$.

from 2 genomic loci, miR-26a-1 and miR-26a-2, residing in the introns of the *CTDSPL* and *CTDSP2* genes (56). Relative expression levels for pri-miR-26a-1 and pri-miR-26a-2 in IFN-α–treated versus untreated islets were 1.5-fold ($P < 0.008$) and 1.3-fold ($P < 0.001$) higher, respectively (Figure 4E), suggesting that IFN-α reduces miR-26a expression not by suppressing its transcription, but rather through enhancing its degradation. A similar effect was observed for the primary miR-22 and miR-29b transcripts in IFN-α–treated human islets (SI Results and Supplemental Figure 9B).

IFN-α affects miR-26a processing through upregulation of PNPT1 exoribonuclease. Because the expression of mature and primary miR-26a transcripts changed in opposite directions, we concluded that miR-26a downregulation by IFN-α is mediated at the posttranscriptional level. Thus, we explored the mechanisms by which IFN-α triggers miR-26a degradation. miR decay involves exonucleolytic degradation through 5′–3′ or 3′–5′ decay pathways (57–59). First, we mined our RNA-seq data set to determine if any known miR-decay-pathway enzymes were regulated by IFN-α. We identified 2 exoribonucleases (*XRN1* and *PNPT1*) that were upregulated by IFN-α. The relative expression levels, as detected by qRT-PCR in 7 IFN-α–treated

compared with untreated islets, were 2.4-fold ($P = 0.001$) for *XRN1* and 11.5-fold ($P = 0.003$) for *PNPT1* (Figure 5A). We also assessed XRN1 and PNPT1 protein expression in cellular lysates from IFN-α–treated islets. Compared with the robust expression of PNPT1, XRN1 was expressed at lower levels in human islets, but the levels of both proteins were increased by IFN-α (Figure 5B). IFN-α treatment also increased *Xrn1* and *Pnpt1* expression in NIT-1 cells (Supplemental Figure 10A).

To determine whether these 2 exoribonucleases are involved in the IFN-α–induced TET2 upregulation via miR-26a degradation, we cotransfected NIT-1 cells with a Luc plasmid containing the *TET2* 3′-UTR, along with constructs expressing either XRN1 or PNPT1. *TET2* 3′-UTR–driven Luc expression was significantly upregulated by PNPT1 overexpression ($P < 0.0007$), but was not affected by XRN1 overexpression (Figure 5C). Consistent with these results, knockdown of *XRN1* or *PNPT1* exoribonucleases in NIT-1 cells by transfection with siRNAs together with pTET2-3′-UTR Luc plasmid resulted in a significantly decreased Luc activity ($P < 0.01$) only when PNPT1 expression was downregulated, but not when XRN1 was inhibited (Figure 5D). These results suggested that upregulation of PNPT1 by IFN-α triggers upregulation of TET2 expression via increased degradation of miR-26a.

To confirm that the PNPT1 regulatory effect on TET2 is indeed mediated through miR-26a, we cotransfected NIT-1 cells with the pTET2-3′-UTR Luc plasmid and miR-26a mimic, with and without constructs expressing XRN1 or PNPT1. The cells overexpressing PNPT1 and mir-26a showed increased Luc activity of the pTET2-3′-UTR Luc plasmid compared with cells expressing miR-26a alone, or with cells expressing XRN1 and miR-26a (Figure 5E and Supplemental Figure 10B). Moreover, infection of human islets with a lentivirus expressing either XRN1 or PNPT1 resulted in significantly reduced miR-26a expression only in islets infected with PNPT1, but not in XRN1 or control EGFP-expressing lentivirus (Figure 5F and Supplemental Figure 10C). Decreased miR-26a expression was correlated with increased expression of *TET2* in the islets infected with PNPT1-expressing lentivirus (Supplemental Figure 10D). Taken together, these findings demonstrate that PNPT1 exoribonuclease mediates IFN-α–induced upregulation of TET2 through downregulation of miR-26a.

IFN-α induces the PNPT1/miR-26a/TET2 cascade in human β cells. We next investigated if the induction of the PNPT1/miR-26a/TET2 cascade is functional in human β cells. We purified human pancreatic β cells from human islet samples incubated with or without IFN-α by fluorescence-activated cell sorting (FACS), using Newport Green DCF Diacetate (NG) dye (60). To check the enrichment of the sorted NG-stained cells in β cells, we assessed insulin (*INS*) and glucagon (*GCG*) mRNA expression in the NG-positive relative to NG-negative cells in 5 IFN-α–treated and untreated samples. The *INS* mean fold change was 56.08 ± 17.41, while the *GCG* mean fold change was 0.5505 ± 0.06 in NG-positive cells compared with NG-negative cells ($P = 0.005$) (Supplemental Table 7), reflecting the significant β cell enrichment of the NG-positive population. We then assessed the *TET2* and *PNPT1* expression levels in NG-positive cells from IFN-α–treated and untreated samples. Both *TET2* and *PNPT1* expression levels were upregulated in IFN-α–treated human β cells relative to untreated cells, with a fold change of 1.8 ± 0.17 for TET2 ($P = 0.0008$) and 14.04 ± 3.9 for PNPT1 ($P = 0.002$) (Figure 6).

IFN-α triggers the development of autoimmune diabetes in transgenic mice overexpressing IFN-α in the islets by upregulating TET2 via the PTNPT1/miR-26a pathway. To confirm our findings in vivo we generated IFNα-INS1^{CreERT2}–transgenic mice, in which β cells express IFN-α upon tamoxifen induction. Figure 7A summarizes the generation of IFNα-INS1^{CreERT2} mice. We first generated the IFN-α mice by targeting a transgenic cassette containing the mouse *IFNα* cDNA, a STOP codon flanked by LoxP sites, and the pCAGGS promoter into the Rosa26 locus (Figure 7A). Generation and characterization of the INS1^{CreERT2} mice was described by Thorens et al. (61). IFNα-INS1^{CreERT2} mice were created by breeding the IFN-α mice with INS1^{CreERT2} mice and they were maintained on the C57BL/6J background. Assessment of IFN-α mRNA expression in islets isolated from IFNα-INS1^{CreERT2} mice, 2 weeks after IFN-α induction, showed a 1,386 ± 315.1-fold increase in transgenic mice compared with 7.686 ± 4.9-fold in their WT littermates ($P = 0.0009$) (Figure 7B). Expression of IFN-α–regulated genes as measured by qRT-PCR was also increased in islets isolated from IFNα-INS1^{CreERT2} mice: *Oas1b*, 6.6 ± 0.4 in transgenic versus 2.3 ± 0.3 in WT mice; *Isg15*, 29.5 ± 5.7 in transgenic versus 9.9 ± 4.2 in WT mice ($P = 0.01$); *Ifit3*, 13.2 ± 2.6 in transgenic versus 3.2 ± 1.1 in WT mice ($P = 0.007$); *Mx2*, 4.6 ± 1.6 in transgenic versus 0.7 ± 0.1 in WT mice ($P = 0.04$) (Supplemental Figure 11).

While only 12% of IFNα-INS1^{CreERT2} mice displayed hyperglycemia (fasting glucose levels > 250 mg/dl) 8 weeks after IFN-α induction, the percentage of hyperglycemic mice increased to 25% after 12 weeks and to 57% after 16 weeks from induction of IFN-α expression in β cells (Figure 7C). The hyperglycemic

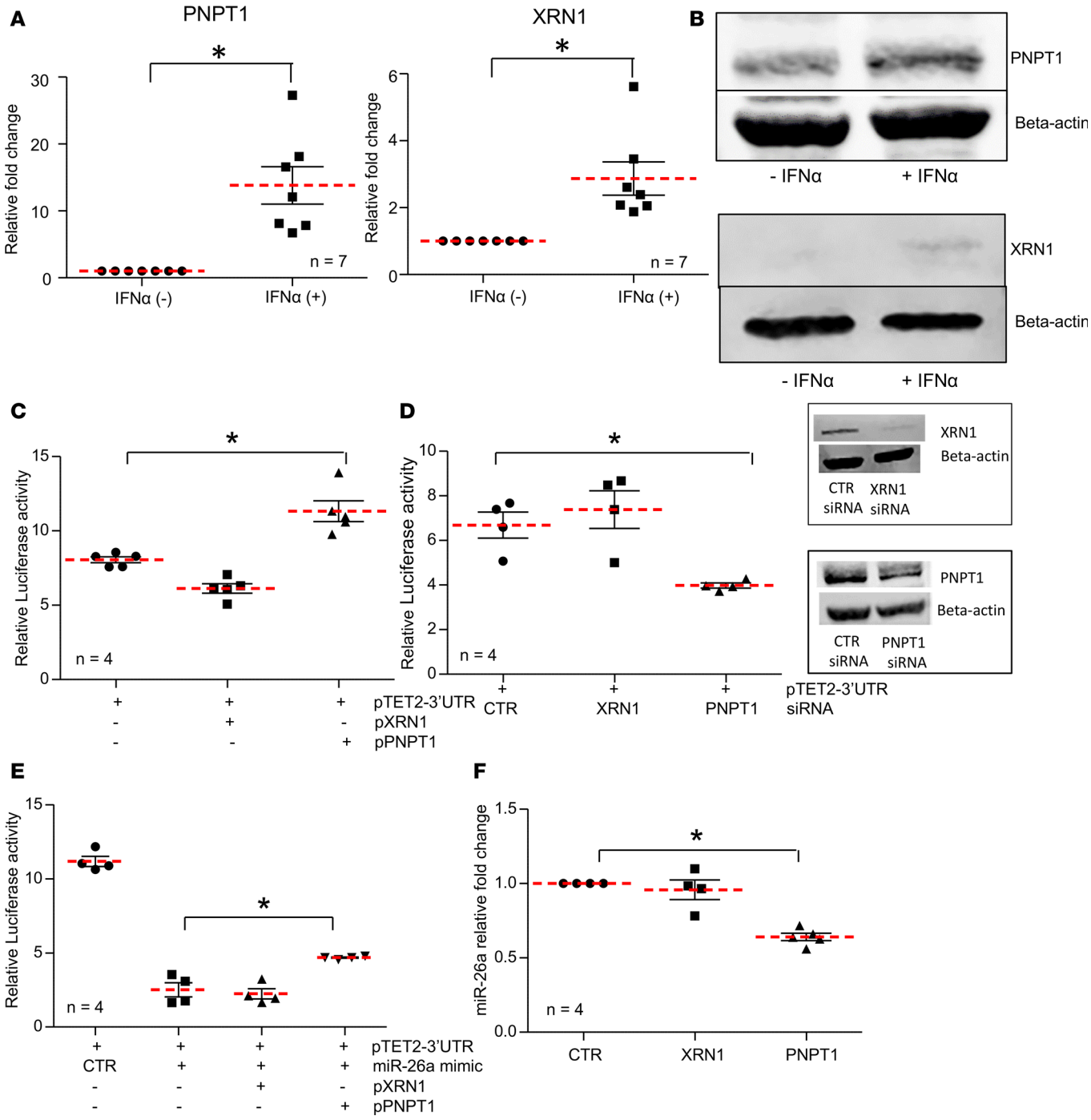

Figure 5. PNPT1 exoribonuclease upregulates expression of TET2 by targeting miR-26a for degradation. (**A**) Relative expression levels of *PNPT1* and *XRN1* mRNA in human islets treated and untreated with IFN-α assessed by qRT-PCR. (**B**) Immunoblotting of PNPT1 and XRN1 proteins in cell lysates from IFN-α–treated and untreated islets. (**C**) Luciferase activity in NIT-1 cells cotransfected with pTET2-3′-UTR Luc plasmid and constructs expressing either XRN1 or PNPT1. (**D**) Luciferase activity in NIT-1 cells cotransfected with pTET2-3′-UTR Luc vector and siRNA for either XRN1 or PNPT1. Boxes represent immunoblotting for XRN1 and PNPT1 proteins in NIT-1 cells treated with XRN1 and PNPT1 siRNA, respectively. Control samples were transfected with control siRNA. (**E**) Luciferase reporter analysis of NIT-1 cells cotransfected with pTET2-3′-UTR Luc construct, miR-26a mimic, and constructs expressing either XRN1 or PNPT1. (**F**) Relative expression levels of miR-26a in human pancreatic islets transduced with lentiviruses expressing either XRN1 or PNPT1. Control islets were transduced with EGFP lentiviral particles. For **C**–**F**, data are representative of 3 independent experiments; results are presented as fold change of quadruplicate samples ± SD. Differences between IFN-α–treated and untreated islets (**A**) and between control and different constructs (**C**–**F**) were determined by *t* test for independent samples. **P* < 0.05.

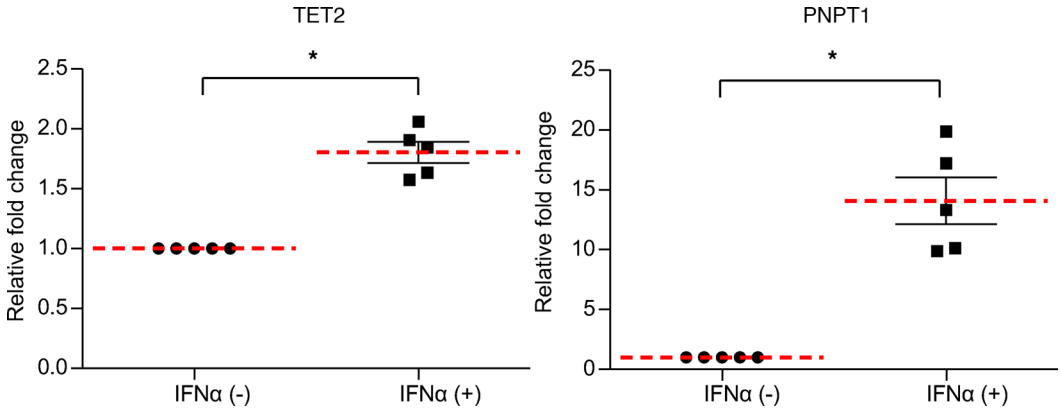

Figure 6. Expression of TET2 and PNPT1 in human β cells. qRT-PCR analysis of *TET2* and *PNPT1* expression in FACS-isolated β cells upon treatment with IFN-α. Results are presented as fold change of mRNA level in IFN-α–treated (+) samples, relative to untreated (–) samples that were considered as having a fold change of 1. Differences between IFN-α–treated and untreated β cells were determined by *t* test for independent samples. **P* < 0.05.

mice had leukocytic infiltration within the islets and many islets appeared irregularly shaped and smaller (Figure 7D). The insulitis was accompanied by a reduced β cell area in diabetic transgenic mice, compared with WT littermates ($P = 0.04$) (Figure 7E). Because not all IFNα-INS1^{CreERT2} mice developed autoimmune diabetes spontaneously, we tested whether the expression of IFN-α in β cells accelerated autoimmune diabetes induced by injections of low-dose streptozotocin (STZ). At day 6 after the first STZ injection, 36% of transgenic mice became diabetic, compared with only 10% of the WT mice (Supplemental Figure 12A). There was no difference in the frequency of diabetes development between transgenic and WT mice starting at day 8 after the first STZ injection (Supplemental Figure 12A). However, mean fasting glucose levels 25 days after the first STZ injection were significantly higher in the IFNα-INS1^{CreERT2} (413.9 ± 33.6 mg/dl) compared with WT mice (261.9 ± 34.3 mg/dl) ($P = 0.003$) (Supplemental Figure 12B), and pancreatic islet area was reduced in transgenic (0.13 ± 0.05) compared with WT (0.21 ± 0.11) ($P = 0.04$) (Supplemental Figure 12C). Average body weight was not different between transgenic and WT mice (Supplemental Figure 12D). These results suggest that IFNα-INS1^{CreERT2} mice are more prone to T1D development, compared with their WT littermates and that IFN-α is a key trigger of islet autoimmunity.

Pancreatic islets isolated from IFNα-INS1^{CreERT2} mice 2–4 weeks after IFN-α β cell induction showed increased levels of 5hmC (0.027 ± 0.006) compared with the WT mice (0.009 ± 0.003) ($P = 0.04$) (Figure 8A). Accordingly, islet expression of *Tet1/2/3* was significantly upregulated (Figure 8B), and miR-26a expression was downregulated (Figure 8C) in transgenic islets. Expression of *Pnpt1* was increased by 1.4 ± 0.1-fold in IFNα-INS1^{CreERT2} mice compared with islets from WT mice ($P = 0.04$) (Figure 8D). Taken together, these results validated the PNPT1/miR-26a/TET2 pathway as a key mechanism in human and mouse β cells for triggering DNA demethylation, upregulation of inflammatory genes, and development of autoimmune diabetes.

Discussion

T1D is caused by autoimmune destruction of the insulin-producing pancreatic β cells (2). A growing body of evidence indicates that pancreatic β cells play a central role in triggering the autoimmune response contributing to their own destruction (3, 62). However, the mechanisms responsible for the deleterious β cell signals that elicit the autoimmune response in T1D are not yet known. We dissected the DNA epigenetic modifications and transcriptomic alterations induced by IFN-α in human pancreatic islets/β cells. Our results point to a β cell–specific mechanism that is triggered by IFN-α, which, through a cascade of events, initiates the inflammatory response in T1D. We focused on IFN-α because of the abundant data pointing to its key role in triggering T1D (15–17).

Most genes we found to be upregulated by IFN-α in human islets are involved in inflammatory, antiviral, and immune response pathways. Moreover, expression of 39 out of 84 IFN-α pathway genes that were found dysregulated in insulitic islets from donors with recent-onset T1D (23) was upregulated in IFN-α–treated islets (e.g., *STAT2*, *IFIT1*, *HLA-a*, *TLR3*, *TAP1*). Several key chemokines known to play an

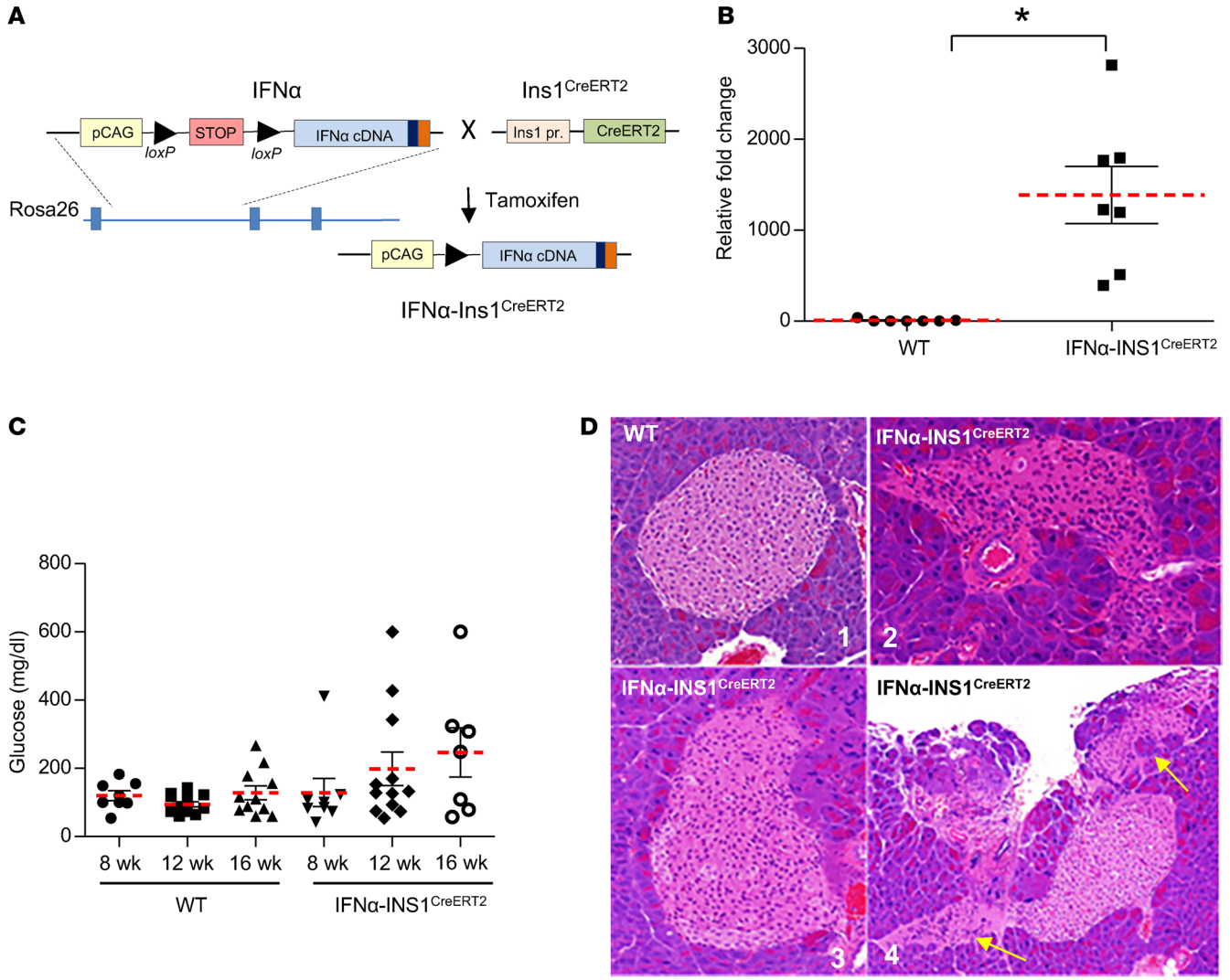

Figure 7. IFN-α expression in β cells triggers autoimmune diabetes in IFNα-INS1^{CreERT2} mice. (**A**) Schematic representation of the generation of IFNα-INS1^{CreERT2} mice: the CAGGS promoter was placed upstream of the mouse IFN-α cDNA and a STOP codon flanked by *loxP* sites was placed between the promoter and IFN-α cDNA. This construct was targeted into the Rosa 26 locus by homologous recombination. The IFN-α mice were crossed with the Ins1^{CreERT2} mice (61) for generation of IFNα-INS1^{CreERT2} mice in which removal of the STOP codon upon tamoxifen injections resulted in IFN-α expression in β cells. (**B**) *IFNα* mRNA expression in pancreatic islets from IFNα-INS1^{CreERT2} and WT mice measured by qRT-PCR. (**C**) Blood glucose concentrations in WT and IFNα-INS1^{CreERT2} mice at 8, 12, and 16 weeks after tamoxifen induction of IFN-α expression. (**D**) Hematoxylin and eosin staining of pancreatic sections from WT and IFNα-INS1^{CreERT2} diabetic mice 12 weeks after induction of IFN-α expression. Arrows indicate irregularly shaped islets in IFNα-INS1^{CreERT2} mice. Original magnification, ×40 (images 1–3) and ×10 (image 4). (**E**) Percentage β cell area relative to pancreatic tissue section in WT versus diabetic IFNα-INS1^{CreERT2} mice at 12–16 weeks after induction of IFN-α expression. Pancreatic sections from WT and IFNα-INS1^{CreERT2} mice; blue represents DAPI-stained nuclei, green represents insulin staining. Original magnification, ×0.6. For **B** and **C**, differences between IFN-α–treated and untreated β cells were determined by *t* test for independent samples. *$P < 0.05$.

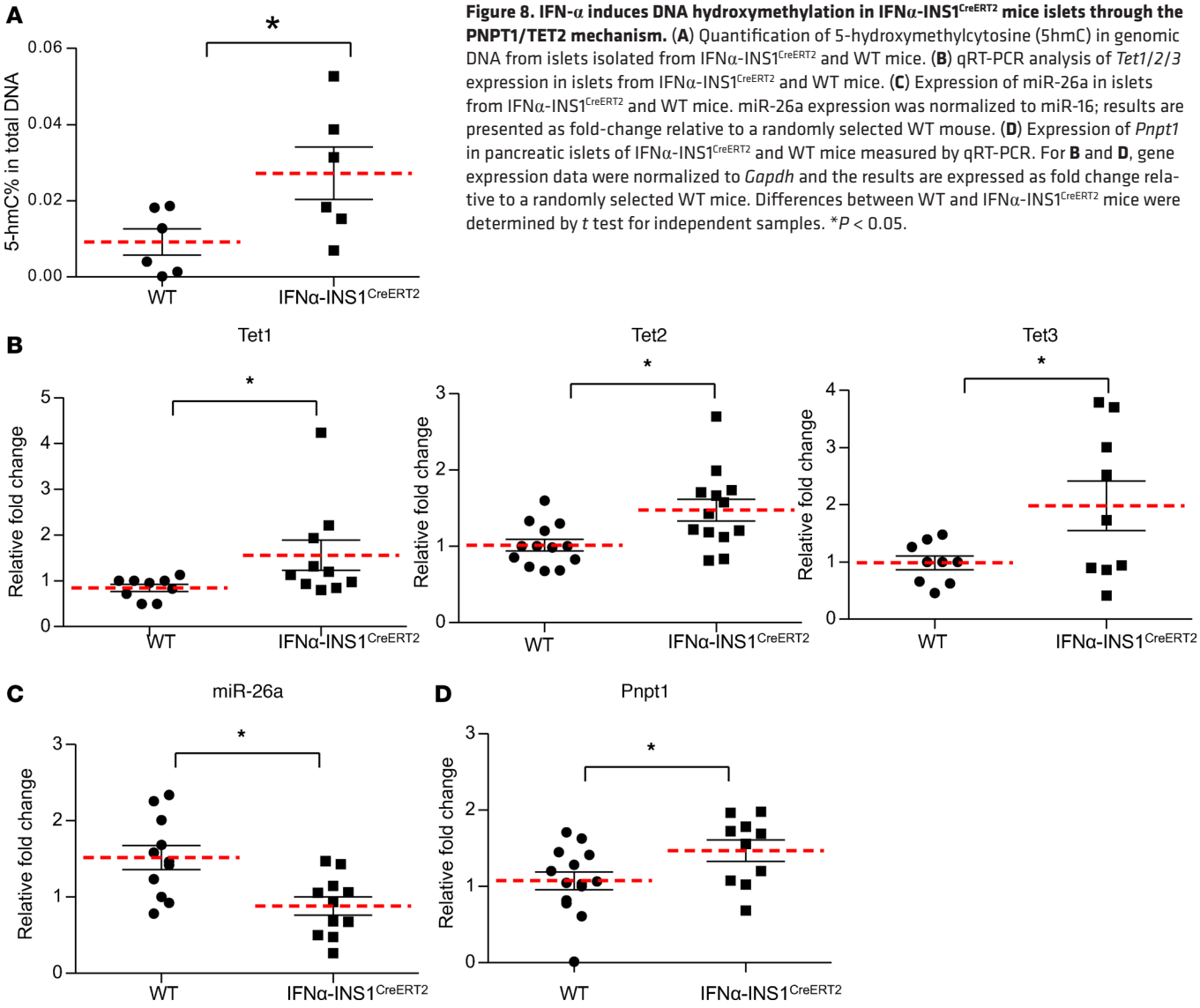

Figure 8. IFN-α induces DNA hydroxymethylation in IFNα-INS1^{CreERT2} mice islets through the PNPT1/TET2 mechanism. (**A**) Quantification of 5-hydroxymethylcytosine (5hmC) in genomic DNA from islets isolated from IFNα-INS1^{CreERT2} and WT mice. (**B**) qRT-PCR analysis of *Tet1/2/3* expression in islets from IFNα-INS1^{CreERT2} and WT mice. (**C**) Expression of miR-26a in islets from IFNα-INS1^{CreERT2} and WT mice. miR-26a expression was normalized to miR-16; results are presented as fold-change relative to a randomly selected WT mouse. (**D**) Expression of *Pnpt1* in pancreatic islets of IFNα-INS1^{CreERT2} and WT mice measured by qRT-PCR. For **B** and **D**, gene expression data were normalized to *Gapdh* and the results are expressed as fold change relative to a randomly selected WT mice. Differences between WT and IFNα-INS1^{CreERT2} mice were determined by *t* test for independent samples. *$P < 0.05$.

important role in the early stages of autoimmune diseases (e.g., *CXCL11*, *CXCL10*, *CCL8*, *CCL18*) (63) were also upregulated by IFN-α in pancreatic islets. Of these, *CXCL10*, the main chemokine overexpressed in the pancreatic islets of recent-onset T1D individuals (23, 64), was the transcript most upregulated by IFN-α. In addition, *IRF-7*, the master transcriptional regulator of the T1D antiviral/inflammatory gene networks in macrophages (65), was predicted by our IPA upstream analysis to regulate most of the transcripts in the IFN-α–treated islets, suggesting that common mechanisms may be shared by immune and β cells to trigger the signals leading to islet inflammation. Importantly, there was a broad overlap between the genes we found overexpressed in IFN-α–stimulated islets and the genes that were recently reported to be upregulated in insulitic pancreases from recent-onset T1D individuals (23). A similar gene expression pattern was found in peripheral blood mononuclear cells (PBMCs) from children genetically predisposed to T1D, prior to T1D onset (21). Moreover, this gene expression pattern was also shown to precede T1D onset in NOD mice (66). Together, these data suggest that expression of IFN-α in pancreatic islets (e.g., during viral infections) is associated with upregulation of genes and pathways that can initiate β cell autoimmunity and therefore T1D development.

Our data showed that many genes within inflammatory and immune pathways were significantly hypomethylated at CpG regions following islet exposure to IFN-α. Our findings are in agreement with studies of other autoimmune diseases that share with T1D a pathology involving activation of type I IFN pathways (67–73). Studies in these diseases demonstrated significant global DNA demethylation

in different cell types, relevant for disease causality. Given the significant DNA hypomethylation detected in IFN-α–treated islets, we tested whether key regulators of DNAm patterns were altered by IFN-α treatment. We found that IFN-α upregulated the expression of TET dioxygenases, especially TET2, and increased 5hmC levels in human islets. Given that TET proteins catalyze conversion of 5mC to 5hmC, the first intermediates of the DNA demethylation processes (50), our results suggest that IFN-α induces DNA demethylation in human islets by a TET-mediated mechanism. Replication-independent TET demethylation mechanisms are mediated by TDG enzymes that remove the subsequent 5hmC oxidation products (5-formylcytosine [5fC] and 5-carboxylcytosine [5caC]), promoting active DNA demethylation (50). Along with upregulation of *TET*s, we also found increased expression of the *TDG* gene, indicating that IFN-α directly triggers active DNA demethylation pathways in pancreatic islets. Consistent with our findings, upregulation of TET proteins has been implicated in the global DNA hypomethylation observed in immune cells from patients with systemic lupus erythematosus (SLE) (74) and rheumatoid arthritis (75), 2 autoimmune diseases associated with the activation of IFN-α. These findings suggest a possible general mechanism in which IFN-α changes the epigenomic landscape in target tissues, in a way that triggers an immune attack on these tissues, thereby leading to autoimmunity.

Our studies revealed that the IFN-α–mediated upregulation of TET2 resulted from alterations in the miR-26a/TET2 regulatory network. In agreement with our results, Fu et al. showed that miR-26a targets the *TET* and *TDG* 3′-UTRs and that *TET1/2/3* and miR-26a expression change in opposite directions during pancreatic cell differentiation (76). We also found that 2 additional miRs were downregulated in IFN-α–treated islets, miR-29b and miR-22, but they had a significantly lower impact on *TET2* 3′-UTR regulation compared with miR-26a. However, it is conceivable that the combined effects of IFN-α–mediated downregulation of miR-26a, miR29b, and miR-22 contributed to the upregulation of *TET2* expression. In fact, more than 30 different miRs were shown to target the *TET2* 3′-UTR and to regulate its expression to varying extents in myeloid leukemia (55). Interestingly, a reverse expression pattern of miR-26a, miR-29b, and miR-22 was found in pancreatic islets exposed to an IL-1β, TNF-α, and IFN-γ cytokine cocktail (77). These results, together with the findings of increased *DNMT3A* and *DNMT3B* levels in islets treated with IL-1β, TNF-α, and IFN-γ (78), suggest that different proinflammatory cytokines (e.g., IFN-α, TNF-α) differentially regulate the epigenome and gene expression and that the DNAm landscape can dynamically change during the disease progression. The IFN-α effects we observed probably reflect the early stages of T1D when triggered by viral infection, since IFN-α is the first cytokine secreted during viral infections. However, when the inflammatory cytokine cascade progresses, other cytokines come into play (e.g., IFN-γ, TNF-α, IL-1β) that may trigger different epigenetic effects.

We found that IFN-α–mediated suppression of miR-26a was regulated at the posttranscriptional level. Two enzymes involved in the miR decay pathway were upregulated by IFN-α in human islets: *XRN1*, an exoribonuclease responsible for the 5′–3′ RNA degradation in the cytoplasmic processing bodies; and *PNPT1*, a 3′–5′ exoribonuclease that mediates RNA degradation in the exosome complex (79). Modulation of *XRN1* levels by IFN-α has not been reported previously. In contrast, studies have shown that *PNPT1* is an early type I IFN response gene, transcriptionally regulated through an IFN-stimulated response element present in its promoter (80). The double-stranded RNA poly(I:C) also stimulates PNPT1 expression, suggesting that viral infections may trigger PNPT1 upregulation, probably through IFN-α (80, 81). Interestingly, our data showed that IFN-α also induced hypomethylation of PNPT1 CpG sites, correlating with its increased expression that we observed in islets exposed to IFN-α. We found downregulation of miR-26a after overexpression of *PNPT1*, but not of *XRN1* in human islets, demonstrating that PNPT1 targets miR-26a for degradation.

To determine if IFN-α activates the PNPT1/miR26a/TET2 mechanism in β cells in vivo, we generated IFNα-INS1^{CreERT2}–transgenic mice with inducible IFN-α expression in β cells. These transgenic mice showed increased incidence of diabetes with time, reaching 57% at 16 weeks after induction of IFN-α expression. It is likely that the lag time from induction of IFN-α expression in β cells to development of diabetes, as well as the fact that not all transgenic mice developed diabetes, may be caused by maintaining the transgenic mice on the C57BL/6J background, a strain that is highly resistant to diabetes. Stewart et al., who developed a transgenic model with constitutive expression of a hybrid human IFN-α gene in β cells, also found that only 5% of the transgenic mice developed diabetes when bred on the inbred C57BL/6J strain, while 50% of the transgenic mice developed diabetes when they were bred on the outbred CD1

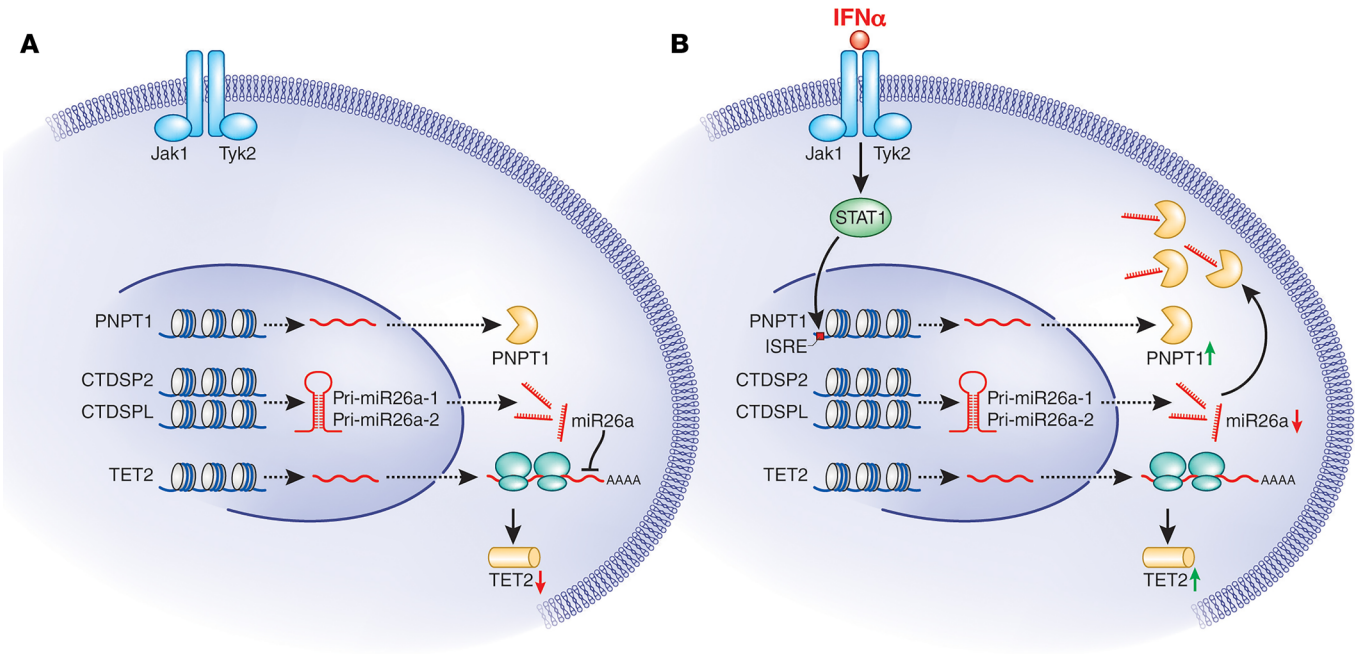

Figure 9. Schematic model for IFN-α regulation of TET2 through PNPT1 and miR-26a.

strain (26). The islet phenotype of the diabetic IFNα-INS1^{CreERT2} mice was similar to the islet phenotype of the transgenic mice with constitutive IFN-α expression (26), including β cell loss and leukocytic infiltration. These results demonstrate that β cell expression of IFN-α triggers a cascade of events that lead to islet pathology resembling the human T1D. Similar to the findings in human islets in vitro, we found increased TET2 expression and 5hmC levels in IFNα-INS1^{CreERT2} islets early after IFN-α induction, and 6–10 weeks before diabetes development in transgenic mice, suggesting that increased DNA hypomethylation may be an early molecular event contributing to diabetes development.

Taken together, our findings suggest a mechanism in which expression of IFN-α in pancreatic islets, during acute or chronic infections, induces upregulation of exonuclease PNPT1, which leads to miR-26a degradation. Reduction of miR-26a expression (and possibly miR-29b and miR-22) alters the posttranscriptional regulation of the *TET2* 3′-UTR, resulting in increased TET2 expression. Overexpression of TET2 in turn increases global 5hmC, leading to DNA demethylation (Figure 9). Changes in DNAm patterns in islets induced by IFN-α could play a causal role in disease etiology. Indeed, epigenetic studies in SLE showed that hypomethylation of IFN-α–regulated genes precedes the IFN-α transcription signature, suggesting that early epigenetic events precede disease onset (82).

Our work addresses key questions about the link between early events affecting pancreatic β cells and the subsequent T1D onset. Viral infections that trigger inflammatory responses in the islets are believed to initiate T1D, likely through local IFN-α production. Our work has pinpointed the IFN-α–responsive pathways causing DNA epigenetic modifications in β cells that in genetically predisposed individuals could trigger an autoimmune attack on the β cells.

Methods

Cell lines and pancreatic islet samples

Cell lines. NIT-1 mouse β cells (derived from a female NOD/Lt mouse) were purchased from ATCC (CRL-2055). The cells were grown in Ham's F12K medium (Gibco) and 10% FBS. The cells were kept at 37°C in 5% CO_2.

Pancreatic islet samples. Deidentified anonymous human islets from 52 donors were obtained through the NIH-supported Integrated Islet Distribution Program (IIDP). Age of the donors ranged from 21 to 59 years; 18 were female and 34 were male. BMI ranged from 20.4 to 38.9. Mean cold ischemia time was 563.7 minutes. Upon arrival, islets were grown for 24 hours in RPMI (Gibco) supplemented with 5.5 mM

glucose and 10% FBS at 37°C in 5% CO_2. After 24 hours, islet samples were stimulated with 2,000 U/ml IFN-α (Millipore) for 24, 48, or 120 hours.

RNA isolation, cDNA synthesis, qRT-PCR, and RT-PCR

Total RNA was isolated using TRIzol (Life Technologies). Genomic DNA was removed by DNAase treatment using an RQ1 RNAase-Free DNAase kit (Promega). First-strand cDNA synthesis was done using a Superscript First-Strand Synthesis System III (Life Technologies).

mRNA expression was measured by real time qRT-PCR using the Applied Biosystems QuantStudio system. mRNA levels of *TET1/2/3*, *TDG*, and *GAPDH* as well as of mouse genes *Isg15*, *Ifit3*, *Oas1b*, *Pnpt1*, *Tet2*, and *Gapdh* were assessed by TaqMan Gene Expression Assay (Applied Biosystems). mRNA levels of human *OAS1*, *SP100*, *IFIH1*, *CD40*, *TLR3*, *IRS1*, *XRN1*, and *PNPT1* genes as well as of mouse *Tet1/2/3*, *Xrn1*, and *Pnpt1* were analyzed using a SYBR Green assay with the primers listed in Supplemental Table 8. Expression levels of pri-miR-26a-1 and -2, pri-miR-29b-1 and -2, and miR-22 were assessed using the TaqMan assay. Results were analyzed by the comparative Ct (ΔΔCt) method. Gene expression was normalized to *GAPDH* for each transcript, and the gene expression in IFN-α–treated samples was calculated relative to untreated samples.

miR expression in human pancreatic islets and NIT-1 cells was quantified by the stem-loop RT-PCR method (83). Total RNA (5 ng) was reverse transcribed with a TaqMan MicroRNA Reverse Transcription Kit using loop primers specific for miR-26a and miR-16 and analyzed by real-time PCR. Results were analyzed by the ΔΔCt method; miR-26a was normalized to miR-16 expression and the expression fold change in IFN-α–treated samples was calculated relative to untreated samples.

Direct sequencing of bisulfate-treated DNA

Methylation status of *GGA3*, *SLC25A31*, *ERAP1*, and *IRF7* genes was determined by cloning and bisulfate sequencing as described previously (38). After bisulfate treatment of DNA using an EZ DNA Methylation-Gold kit (Zymo Research), bisulfate-treated DNA was amplified using the primers listed in Supplemental Table 8. PCR products were cloned using TOPO TA cloning kit (Life Technologies). DNA was sequenced using an ABI 3130 Genetic Analyzer. For each analyzed gene, a minimum of 10 clones from each sample (treated and untreated with IFN-α) were sequenced and their methylation status was determined based on protection from conversion of cytosine to uracil residues.

Western blot analyses

Total proteins were extracted from either pancreatic islet samples or NIT-1 cells as described previously (84). Cell lysates were quantified using a Pierce BCA Protein Assay kit (Thermo Fisher Scientific) and equal amounts of total protein extracts (50–80 μg) were separated by sodium dodecyl sulfate–polyacrylamide gel electrophoresis and transferred to Immobilon-P membranes (Millipore). After a 1-hour incubation in Odyssey Blocking Buffer (Li-COR), membranes were blotted overnight at 4°C with the following primary antibodies: anti-XRN1 (Abcam, ab70259) (1:5,000), anti-PNPT1 (Abcam, ab157109) (1:1,000), anti-TET2 (Diagenode, C15200179) (1:1,000), and anti–β-actin (Cell Signaling Technology, 14B7) (1:1,000). The primary antibodies were detected using goat anti-mouse (926-32210) and goat anti-rabbit (926-68071) secondary antibodies (Li-COR) (1:5,000) and the immunoblots were visualized using the Li-COR Odyssey system.

5hmC quantification and TET hydroxylase activity

Genomic DNA was extracted from human pancreatic islets treated and untreated with IFN-α using an ArchivePure DNA Cell/Tissue Kit (5 Prime). Global DNA hydroxymethylation was quantified using the Hydroxymethylated DNA Quantification kit (Abcam) according to the manufacturer's protocol. The absorbance end point was read on a FLUOstar Omega (BMG Labtech) microplate reader at 450 nm and the percentage of 5hmC in total DNA was calculated based on the formula provided in the manufacturer's protocol.

TET nuclear proteins were extracted using NE-PER Nuclear and Cytoplasmic Extraction Reagents (Thermo Fisher Scientific), and quantified by a Pierce BCA Protein Assay kit. TET activity was measured using a TET Hydroxylase Activity Quantification kit (Abcam) according to the manufacturer's protocol. The absorbance was read on a FLUOstar Omega microplate reader at 450 nm and TET activity (OD/ng/min) was calculated according to the manufacturer's protocol.

siRNA-mediated inhibition of XRN1 and PNPT1

NIT-1 cells were grown in 24-well plates for 24 hours and cotransfected with *TET2* 3′-UTR Luc plasmid (GeneCopoeia) and with XRN1 and PNPT1 Silencer Select siRNAs (Ambion) to a final concentration of 500 μg and 10 nM, respectively, using Lipofectamine 3000 transfection reagent (Life Technologies). Cells cotransfected with *TET2* 3′-UTR and Silencer Select Negative Control (Ambion) were used as negative controls. Cells were harvested 48 hours after transfection and luciferase activity was measured using the Dual-Luciferase Reporter assay System (Promega). Luciferase activity was expressed as the ratio of firefly to Renilla luciferase values.

Overexpression of PNPT1 and XRN1 in NIT-1 cells and human pancreatic islets

Overexpression of PNPT1 and XRN1 in NIT-1 cells by transfection. NIT-1 cells were cotransfected with *TET2* 3′-UTR Luc plasmid together with XRN1 and PNPT1 cDNA plasmids (GeneCopoeia), to a final concentration of 200 μg for each plasmid, using FuGENE HD transfection reagent (Promega). Cells were harvested 48 hours after transfection and luciferase activity was measured using the Dual-Luciferase Reporter assay System.

Overexpression of PNPT1 and XRN1 in human pancreatic islets by transduction. Lentiviral vectors (Lv105) containing PNPT1 and XRN1 ORFs as well as the purified lentiviral particles were generated at GeneCopoeia, with a concentration of 4.29×10^8 transducing units (TU)/ml for LPP-LV105-PNPT1 and 9.28×10^8 TU/ml for LPP-Lv105-XRN1. Islets transduced with EGFP Lentifect purified lentiviral particles (LPP-EGFP-Lv105) (GeneCopoeia) were used as negative controls. Groups of 200 pancreatic islets were dispersed using Accutase and 3×10^5 cells were infected with LV105-PNPT1, LV105-XRN1, or LV105-EGFP (2.1×10^5 to 3×10^5 TU) for 2 hours in 200 μl of serum-free RPMI 1640 medium at 37°C. Following incubation, 800 μl of complete medium was added and the samples were further incubated for 48 hours at 37°C.

DNAm and data analysis

DNA was extracted from islet samples treated or untreated with IFN-α, and was subjected to methylation analysis using the Illumina 450K methyl BeadChip as we previously described (38). Briefly, after raw intensity data were extracted from the chips and quantile-normalized, the methylation level for each probe was calculated in GenomeStudio (Illumina). The methylation data were processed with open source R package IMA and MEDME (http://bioonductor.org). First, after data filtering, only the sites on autosomal chromosomes with a significant detection *P* value less than 0.001 were kept for downstream analysis and then the β was converted to log2 ratio of β value to (1 – β) value (85). The differentially methylated sites in IFN-α–stimulated cells were identified by paired LIMMA test at *P* value less than 0.05 and at least 10% methylation level change. The distribution of differentially methylated (hypo- or hypermethylated) sites located in various genomic regions was investigated and the functions of genes that harbor these methylation sites were evaluated with GO enrichment analysis. The methylation profiles were also correlated with gene expression profiles to identify the differentially expressed genes with methylation level changes. Data were deposited into the NCBI's Gene Expression Omnibus (GEO) database (reference series GSE124811, accession number GSE124809).

RNA-seq

Sequencing. Total RNA from islets treated and untreated with IFN-α was extracted using TRIzol. RNA-seq and data analysis were performed as previously described (37, 86). The cDNA library was prepared using Illumina TruSeq RNA Sample Prep Kits. Next-generation sequencing was performed on an Illumina HiSeq 2000 using the Single-Read Cluster Generation kit v2 and SBS Sequencing kit v3. Image analysis and base calling were conducted using SDS 2.5/RTA1.5 software (Illumina). Data were deposited in into the NCBI's GEO database (reference series GSE124811, accession number GSE124810).

Data analysis. The reads with good quality were aligned to several human reference databases including hg19 human genome, exon, splicing-junction segments, and contamination database including ribosome and mitochondrial sequences using the BWA alignment algorithm. After filtering reads mapped to the contamination database, the reads that were uniquely aligned to the exon and splicing-junction segments with maximal 2 mismatches for each transcript were then counted as expression level for the corresponding transcripts. The read counts were log2 transformed and normalized at an equal global median value in order to compare transcription levels across samples. The differential analysis by DEGseq was performed to identify significantly dysregulated genes at FDR-adjusted *P* value of less than 0.05 in all 3 IFN-α–treated islets compared with paired untreated islets (87).

Pathway analysis. Differentially expressed transcripts were subjected to pathway analysis by GO. Fisher's exact test was used to calculate *P* values for the probability that a pathway was significantly enriched in input genes compared with the genome. Genes differentially expressed between IFN-α–treated and untreated islets were also analyzed by IPA (Qiagen). Functions and pathways with *P* value less than 0.05 (Fisher's exact test) were considered to be statistically significant. IPA's upstream regulator was used to identify potential transcriptional regulators for IFN-α–induced genes. Fisher's exact test *P* value was used to assess the significance of enrichment of the gene expression data for the genes downstream of the transcriptional regulator.

FACS isolation of human β cells

Islets were dispersed using Accutase and cells were cultured in RPMI 1640 supplemented with 10% FBS at 37°C. Half of the cells were treated with 2,000 U/ml IFN-α (Millipore), while the other half were kept in media and used as controls. After 24 hours, islet cells were incubated with 20 μM Newport Green DCF Diacetate (NG) at 37°C for 30 minutes, protected from light. Prior to flow cytometry, labeled cells were washed twice with FACS buffer (PBS, 4% FBS) and transferred into 35-μm nylon mesh cell strainer–capped tubes (BD Biosciences). DNase (1 mg/ml) and 3 μM DAPI were added to the FACS buffer before the sorting. Sorting was done on a FACSAria (BD Biosciences).

Generation of IFNα-INS1^{CreERT2} mice

The targeting construct and IFN-α mice were created by inGenious Targeting Laboratory. The IFN-α sequence was subcloned into the *Mlu*I site of ROSA26-pCAG-stop backbone vector. The stop cassette in the ROSA-stop vector contained a floxed PGK/gb2neoPGKpolyA2A2XSV40pa cassette. The pCAGGS promoter was placed upstream of the floxed cassette and the BGH poly A sequence was placed at the 3′ end of the IFN-α sequence. The targeting vector contained a 1.8-kb homology arm with ROSA26 genomic sequence upstream of the pCAGGS promoter and a 4.34-kb ROSA26 homology arm downstream of the BGHpA sequence. The targeting vector was confirmed by restriction enzyme digestion and sequencing. The targeted construct was linearized and electroporated into 129/Sv × C57BL/6J embryonic stem cells. The targeted positive clones were identified by Southern blotting and direct sequencing. Targeted clones were injected into C57BL/6J blastocysts. Resulting chimeras with high percentage agouti color were mated to C57BL/6J mice to generate F1 heterozygous offspring. Tail DNA was analyzed by PCR. The IFN-α mice were bred with INS1^{CreERT2} mice (Jackson Laboratories), generated as described in Thorens et al. (61) and the resulting IFNα-INS1^{CreERT2} mice were maintained on the C57BL/6J background. Recombination and IFN-α expression was induced in 10-week-old IFNα-INS1^{CreERT2} mice by i.p. injection of 2 mg tamoxifen 4 times over a 2-week period.

Acceleration of T1D in IFNα-INS1^{CreERT2} by administration of multiple low doses of STZ

Two weeks after induction of IFN-α expression by tamoxifen injections, IFNα-INS^{CreERT2} and WT mice were i.p. injected for 5 consecutive days with 40 mg/kg STZ (Sigma-Aldrich). Urine glucose was measured using chemstrip 5 OB (Roche Diagnostics) before STZ administration, on days 6, 8, and 10. Mice were euthanized 25 days after STZ administration, pancreata were harvested for histological evaluation, and blood glucose was measured using a glucose meter (Roche Diagnostics). A mouse was considered diabetic if it had 2 consecutive glucose readings of 250 mg/dl or higher.

Tissue histology and immunofluorescence procedures

Pancreata from IFNα-INS1^{CreERT2} mice were harvested and tissues were fixed in 10% formalin solution and embedded in paraffin. Sections (5 μm) were stained with hematoxylin and eosin and 4 sections per mouse were examined after the slides were scanned using a 3DHistech Pannoramic 250 Flash II Slide Scanner. For immunofluorescence of islet insulin, slides were deparaffinized and rehydrated before applying the primary antibody, a rabbit monoclonal antibody against insulin (ab181547, Abcam). Five slides from each mouse were scanned using the 3DHistech P250 High Capacity Slide Scanner and β cell area was assessed in CaseViewer software.

Statistics

Differences in continuous parameters between control and treated samples or between control and transgenic mice were analyzed using the *t* test for independent samples and a 2-tailed *P* value was used. *P* less than 0.05 was considered significant.

Study approval

Islets from 52 donors were obtained through the NIH-supported IIDP. Islets were received as deidentified anonymous samples, and the project was approved by the Albert Einstein College of Medicine IRB as exempt (IRB protocol 2016-2668). Mouse studies were approved by the Albert Einstein College of Medicine Institutional Animal Care and Use Committee.

Author contributions

MSL and YT designed the study and wrote the manuscript. MSL, EK, LC, and AE performed experiments. ZY and WZ performed bioinformatical analysis.

Acknowledgments

We thank Lori Sussel for helpful discussions. We are also grateful to Andrew Stewart and Aaron Bender for providing valuable reagents and for helpful advice and to Larissa Fausitino for technical advice. We thank Pierre Chambon (Institute of Genetics and Molecular and Cellular Biology, France) for providing us the B6(Cg)-Ins1$^{tm2.1(cre/ERT2)Thor}$/J (INS1$^{Cre/ERT2}$) mice through the Jackson Laboratories. This work was supported in part by grants DK061659, DK067555, and DK073681 from the National Institute of Diabetes and Digestive and Kidney Diseases and VA Biomedical Laboratory Research and Development Merit Award 1I01BX002031 (to YT). The National Cancer Institute's cancer center support grant P30CA013330 partially supported work that was done through the Analytical Imaging Facility and Flow Cytometry Core Facility. The 3DHistech Pannoramic 250 Flash II Slide Scanner was purchased using the Shared Instrumentation Grant 1S10OD019961-01.

Address correspondence to: Mihaela Stefan-Lifshitz, Albert Einstein College of Medicine, Forchheimer 702, 1300 Morris Park Avenue, Bronx, New York, 10461, USA. Phone: 718.430.8530; Email: mihaela.stefan@einstein.yu.edu.

1. Hasham A, Tomer Y. The recent rise in the frequency of type 1 diabetes: who pulled the trigger? *J Autoimmun*. 2011;37(1):1–2.
2. Atkinson MA, Eisenbarth GS, Michels AW. Type 1 diabetes. *Lancet*. 2014;383(9911):69–82.
3. Soleimanpour SA, Stoffers DA. The pancreatic β cell and type 1 diabetes: innocent bystander or active participant? *Trends Endocrinol Metab*. 2013;24(7):324–331.
4. Storling J, Brorsson CA. Candidate genes expressed in human islets and their role in the pathogenesis of type 1 diabetes. *Curr Diab Rep*. 2013;13(5):633–641.
5. Fløyel T, Kaur S, Pociot F. Genes affecting β-cell function in type 1 diabetes. *Curr Diab Rep*. 2015;15(11):97.
6. Størling J, Pociot F. Type 1 diabetes candidate genes linked to pancreatic islet cell inflammation and beta-cell apoptosis. *Genes (Basel)*. 2017;8(2):E72.
7. Osmai M, et al. MicroRNAs as regulators of beta-cell function and dysfunction. *Diabetes Metab Res Rev*. 2016;32(4):334–349.
8. Roggli E, et al. Involvement of microRNAs in the cytotoxic effects exerted by proinflammatory cytokines on pancreatic beta-cells. *Diabetes*. 2010;59(4):978–986.
9. Grieco FA, et al. MicroRNAs miR-23a-3p, miR-23b-3p, and miR-149-5p regulate the expression of proapoptotic BH3-only proteins DP5 and PUMA in human pancreatic β-cells. *Diabetes*. 2017;66(1):100–112.
10. Rhode A, et al. Islet-specific expression of CXCL10 causes spontaneous islet infiltration and accelerates diabetes development. *J Immunol*. 2005;175(6):3516–3524.
11. Tanaka S, et al. Enterovirus infection, CXC chemokine ligand 10 (CXCL10), and CXCR3 circuit: a mechanism of accelerated beta-cell failure in fulminant type 1 diabetes. *Diabetes*. 2009;58(10):2285–2291.
12. Diana J, Lehuen A. Macrophages and β-cells are responsible for CXCR2-mediated neutrophil infiltration of the pancreas during autoimmune diabetes. *EMBO Mol Med*. 2014;6(8):1090–1104.
13. Citro A, Cantarelli E, Piemonti L. The CXCR1/2 pathway: involvement in diabetes pathophysiology and potential target for T1D interventions. *Curr Diab Rep*. 2015;15(10):68.
14. Cnop M, Welsh N, Jonas JC, Jörns A, Lenzen S, Eizirik DL. Mechanisms of pancreatic beta-cell death in type 1 and type 2 diabetes: many differences, few similarities. *Diabetes*. 2005;54 Suppl 2:S97–S107.
15. Grishman EK, White PC, Savani RC. Toll-like receptors, the NLRP3 inflammasome, and interleukin-1β in the development and progression of type 1 diabetes. *Pediatr Res*. 2012;71(6):626–632.
16. Newby BN, Mathews CE. Type I interferon is a catastrophic feature of the diabetic islet microenvironment. *Front Endocrinol (Lausanne)*. 2017;8:232.

17. Lombardi A, Tsomos E, Hammerstad SS, Tomer Y. Interferon alpha: The key trigger of type 1 diabetes. *J Autoimmun*. 2018;94:7–15.
18. Huang X, et al. Interferon expression in the pancreases of patients with type I diabetes. *Diabetes*. 1995;44(6):658–664.
19. Planas R, et al. Gene expression profiles for the human pancreas and purified islets in type 1 diabetes: new findings at clinical onset and in long-standing diabetes. *Clin Exp Immunol*. 2010;159(1):23–44.
20. Foulis AK, Farquharson MA, Meager A. Immunoreactive alpha-interferon in insulin-secreting beta cells in type 1 diabetes mellitus. *Lancet*. 1987;2(8573):1423–1427.
21. Ferreira RC, et al. A type I interferon transcriptional signature precedes autoimmunity in children genetically at risk for type 1 diabetes. *Diabetes*. 2014;63(7):2538–2550.
22. Kallionpää H, et al. Innate immune activity is detected prior to seroconversion in children with HLA-conferred type 1 diabetes susceptibility. *Diabetes*. 2014;63(7):2402–2414.
23. Lundberg M, Krogvold L, Kuric E, Dahl-Jørgensen K, Skog O. Expression of interferon-stimulated genes in insulitic pancreatic islets of patients recently diagnosed with type 1 diabetes. *Diabetes*. 2016;65(10):3104–3110.
24. Fabris P, Floreani A, Tositti G, Vergani D, De Lalla F, Betterle C. Type 1 diabetes mellitus in patients with chronic hepatitis C before and after interferon therapy. *Aliment Pharmacol Ther*. 2003;18(6):549–558.
25. Guerci AP, et al. Onset of insulin-dependent diabetes mellitus after interferon-alfa therapy for hairy cell leukaemia. *Lancet*. 1994;343(8906):1167–1168.
26. Stewart TA, Hultgren B, Huang X, Pitts-Meek S, Hully J, MacLachlan NJ. Induction of type I diabetes by interferon-alpha in transgenic mice. *Science*. 1993;260(5116):1942–1946.
27. Li Q, Xu B, Michie SA, Rubins KH, Schreriber RD, McDevitt HO. Interferon-alpha initiates type 1 diabetes in nonobese diabetic mice. *Proc Natl Acad Sci USA*. 2008;105(34):12439–12444.
28. Marro BS, Ware BC, Zak J, de la Torre JC, Rosen H, Oldstone MB. Progression of type 1 diabetes from the prediabetic stage is controlled by interferon-α signaling. *Proc Natl Acad Sci USA*. 2017;114(14):3708–3713.
29. Lombardi A, Tomer Y. Interferon alpha impairs insulin production in human beta cells via endoplasmic reticulum stress. *J Autoimmun*. 2017;80:48–55.
30. Marroqui L, et al. Interferon-α mediates human beta cell HLA class I overexpression, endoplasmic reticulum stress and apoptosis, three hallmarks of early human type 1 diabetes. *Diabetologia*. 2017;60(4):656–667.
31. MacFarlane AJ, Strom A, Scott FW. Epigenetics: deciphering how environmental factors may modify autoimmune type 1 diabetes. *Mamm Genome*. 2009;20(9-10):624–632.
32. Furey TS, Sethupathy P. Genetics. Genetics driving epigenetics. *Science*. 2013;342(6159):705–706.
33. McVicker G, et al. Identification of genetic variants that affect histone modifications in human cells. *Science*. 2013;342(6159):747–749.
34. Heinz S, et al. Effect of natural genetic variation on enhancer selection and function. *Nature*. 2013;503(7477):487–492.
35. Tammen SA, Friso S, Choi SW. Epigenetics: the link between nature and nurture. *Mol Aspects Med*. 2013;34(4):753–764.
36. Stefan M, et al. Novel variant of thyroglobulin promoter triggers thyroid autoimmunity through an epigenetic interferon alpha-modulated mechanism. *J Biol Chem*. 2011;286(36):31168–31179.
37. Stefan M, et al. Genetic-epigenetic dysregulation of thymic TSH receptor gene expression triggers thyroid autoimmunity. *Proc Natl Acad Sci USA*. 2014;111(34):12562–12567.
38. Stefan M, Zhang W, Concepcion E, Yi Z, Tomer Y. DNA methylation profiles in type 1 diabetes twins point to strong epigenetic effects on etiology. *J Autoimmun*. 2014;50:33–37.
39. Paul DS, et al. Increased DNA methylation variability in type 1 diabetes across three immune effector cell types. *Nat Commun*. 2016;7:13555.
40. Elboudwarej E, et al. Hypomethylation within gene promoter regions and type 1 diabetes in discordant monozygotic twins. *J Autoimmun*. 2016;68:23–29.
41. Rakyan VK, et al. Identification of type 1 diabetes-associated DNA methylation variable positions that precede disease diagnosis. *PLoS Genet*. 2011;7(9):e1002300.
42. Fradin D, et al. Association of the CpG methylation pattern of the proximal insulin gene promoter with type 1 diabetes. *PLoS One*. 2012;7(5):e36278.
43. Chen Z, et al. Epigenomic profiling reveals an association between persistence of DNA methylation and metabolic memory in the DCCT/EDIC type 1 diabetes cohort. *Proc Natl Acad Sci USA*. 2016;113(21):E3002–E3011.
44. Young JI, Züchner S, Wang G. Regulation of the epigenome by vitamin C. *Annu Rev Nutr*. 2015;35:545–564.
45. Reddy MA, Tak Park J, Natarajan R. Epigenetic modifications in the pathogenesis of diabetic nephropathy. *Semin Nephrol*. 2013;33(4):341–353.
46. Keating ST, El-Osta A. Epigenetic changes in diabetes. *Clin Genet*. 2013;84(1):1–10.
47. Lombardi A, Tomer Y. Interferon alpha impairs insulin production in human beta cells via endoplasmic reticulum stress. *J Autoimmun*. 2017;80:48–55.
48. Hamidi T, Singh AK, Chen T. Genetic alterations of DNA methylation machinery in human diseases. *Epigenomics*. 2015;7(2):247–265.
49. van der Wijst MG, Venkiteswaran M, Chen H, Xu GL, Plösch T, Rots MG. Local chromatin microenvironment determines DNMT activity: from DNA methyltransferase to DNA demethylase or DNA dehydroxymethylase. *Epigenetics*. 2015;10(8):671–676.
50. Kohli RM, Zhang Y. TET enzymes, TDG and the dynamics of DNA demethylation. *Nature*. 2013;502(7472):472–479.
51. Zhao B, et al. Redox-active quinones induces genome-wide DNA methylation changes by an iron-mediated and Tet-dependent mechanism. *Nucleic Acids Res*. 2014;42(3):1593–1605.
52. Thienpont B, et al. Tumour hypoxia causes DNA hypermethylation by reducing TET activity. *Nature*. 2016;537(7618):63–68.
53. Ploumakis A, Coleman ML. OH, the places you'll go! Hydroxylation, gene expression, and cancer. *Mol Cell*. 2015;58(5):729–741.
54. Tu J, Liao J, Luk AC, Tang NL, Chan WY, Lee TL. MicroRNAs mediated targeting on the Yin-yang dynamics of DNA methylation in disease and development. *Int J Biochem Cell Biol*. 2015;67:115–120.
55. Cheng J, et al. An extensive network of TET2-targeting microRNAs regulates malignant hematopoiesis. *Cell Rep*. 2013;5(2):471–481.

56. Zhu Y, et al. MicroRNA-26a/b and their host genes cooperate to inhibit the G1/S transition by activating the pRb protein. *Nucleic Acids Res*. 2012;40(10):4615–4625.
57. Towler BP, Jones CI, Newbury SF. Mechanisms of regulation of mature miRNAs. *Biochem Soc Trans*. 2015;43(6):1208–1214.
58. Sokhi UK, et al. Human polynucleotide phosphorylase (hPNPaseold-35): should I eat you or not--that is the question? *Adv Cancer Res*. 2013;119:161–190.
59. Bail S, et al. Differential regulation of microRNA stability. *RNA*. 2010;16(5):1032–1039.
60. Nica AC, et al. Cell-type, allelic, and genetic signatures in the human pancreatic beta cell transcriptome. *Genome Res*. 2013;23(9):1554–1562.
61. Thorens B, Tarussio D, Maestro MA, Rovira M, Heikkilä E, Ferrer J. Ins1(Cre) knock-in mice for beta cell-specific gene recombination. *Diabetologia*. 2015;58(3):558–565.
62. Eizirik DL, Grieco FA. On the immense variety and complexity of circumstances conditioning pancreatic β-cell apoptosis in type 1 diabetes. *Diabetes*. 2012;61(7):1661–1663.
63. Rotondi M, Chiovato L, Romagnani S, Serio M, Romagnani P. Role of chemokines in endocrine autoimmune diseases. *Endocr Rev*. 2007;28(5):492–520.
64. Roep BO, et al. Islet inflammation and CXCL10 in recent-onset type 1 diabetes. *Clin Exp Immunol*. 2010;159(3):338–343.
65. Heinig M, et al. A trans-acting locus regulates an anti-viral expression network and type 1 diabetes risk. *Nature*. 2010;467(7314):460–464.
66. Ban Y, Greenberg DA, Davies TF, Jacobson E, Concepcion E, Tomer Y. 'Linkage analysis of thyroid antibody production: evidence for shared susceptibility to clinical autoimmune thyroid disease. *J Clin Endocrinol Metab*. 2008;93(9):3589–3596.
67. Higgs BW, et al. Patients with systemic lupus erythematosus, myositis, rheumatoid arthritis and scleroderma share activation of a common type I interferon pathway. *Ann Rheum Dis*. 2011;70(11):2029–2036.
68. Zhang Y, Zhao M, Sawalha AH, Richardson B, Lu Q. Impaired DNA methylation and its mechanisms in CD4(+)T cells of systemic lupus erythematosus. *J Autoimmun*. 2013;41:92–99.
69. Absher DM, et al. Genome-wide DNA methylation analysis of systemic lupus erythematosus reveals persistent hypomethylation of interferon genes and compositional changes to $CD4^+$ T-cell populations. *PLoS Genet*. 2013;9(8):e1003678.
70. Ulff-Moller CJ, et al. Twin DNA methylation profiling reveals flare-dependent interferon signature and B cell promoter hypermethylation in systemic lupus erythematosus. *Arthritis Rheumatol*. 2018;70(6):878–890.
71. Imgenberg-Kreuz J, et al. DNA methylation mapping identifies gene regulatory effects in patients with systemic lupus erythematosus. *Ann Rheum Dis*. 2018;77(5):736–743.
72. Yuan FL, Li X, Xu RS, Jiang DL, Zhou XG. DNA methylation: roles in rheumatoid arthritis. *Cell Biochem Biophys*. 2014;70(1):77–82.
73. Imgenberg-Kreuz J, et al. Genome-wide DNA methylation analysis in multiple tissues in primary Sjögren's syndrome reveals regulatory effects at interferon-induced genes. *Ann Rheum Dis*. 2016;75(11):2029–2036.
74. Zhao M, et al. Increased 5-hydroxymethylcytosine in CD4(+) T cells in systemic lupus erythematosus. *J Autoimmun*. 2016;69:64–73.
75. de Andres MC, et al. Assessment of global DNA methylation in peripheral blood cell subpopulations of early rheumatoid arthritis before and after methotrexate. *Arthritis Res Ther*. 2015;17:233.
76. Fu X, et al. MicroRNA-26a targets ten eleven translocation enzymes and is regulated during pancreatic cell differentiation. *Proc Natl Acad Sci USA*. 2013;110(44):17892–17897.
77. Bravo-Egana V, et al. Inflammation-mediated regulation of microRNA expression in transplanted pancreatic islets. *J Transplant*. 2012;2012:723614.
78. Rui J, Deng S, Lebastchi J, Clark PL, Usmani-Brown S, Herold KC. Methylation of insulin DNA in response to proinflammatory cytokines during the progression of autoimmune diabetes in NOD mice. *Diabetologia*. 2016;59(5):1021–1029.
79. Zhang Z, Qin YW, Brewer G, Jing Q. MicroRNA degradation and turnover: regulating the regulators. *Wiley Interdiscip Rev RNA*. 2012;3(4):593–600.
80. Leszczyniecka M, Su ZZ, Kang DC, Sarkar D, Fisher PB. Expression regulation and genomic organization of human polynucleotide phosphorylase, hPNPase(old-35), a type I interferon inducible early response gene. *Gene*. 2003;316:143–156.
81. Sarkar D, Fisher PB. Human polynucleotide phosphorylase (hPNPase old-35): an RNA degradation enzyme with pleiotrophic biological effects. *Cell Cycle*. 2006;5(10):1080–1084.
82. Teruel M, Sawalha AH. Epigenetic variability in systemic lupus erythematosus: What we learned from genome-wide DNA methylation studies. *Curr Rheumatol Rep*. 2017;19(6):32.
83. Chen C, et al. Real-time quantification of microRNAs by stem-loop RT-PCR. *Nucleic Acids Res*. 2005;33(20):e179.
84. Lee HJ, et al. CD40 signaling in Graves disease is mediated through canonical and noncanonical thyroidal nuclear factor κB activation. *Endocrinology*. 2017;158(2):410–418.
85. Wang D, et al. IMA: an R package for high-throughput analysis of Illumina's 450K Infinium methylation data. *Bioinformatics*. 2012;28(5):729–730.
86. Akeno N, et al. IFN-α mediates the development of autoimmunity both by direct tissue toxicity and through immune cell recruitment mechanisms. *J Immunol*. 2011;186(8):4693–4706.
87. Wang L, Feng Z, Wang X, Wang X, Zhang X. DEGseq: an R package for identifying differentially expressed genes from RNA-seq data. *Bioinformatics*. 2010;26(1):136–138.